Defence Research and Development Canada   Recherche et développement pour la défense Canada

DEFENCE R&D DÉFENSE

Appendage and Viscous Forces for Ship Motions in Waves

Kevin McTaggart

Defence R&D Canada – Atlantic

Canada

This page intentionally left blank.

Appendage and Viscous Forces for Ship Motions in Waves
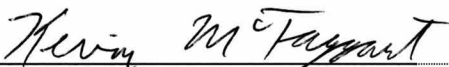
Kevin McTaggart

Defence R&D Canada – Atlantic

Technical Memorandum

DRDC Atlantic TM 2004-227

September 2004
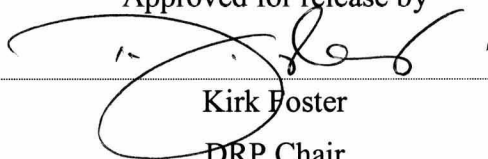
Author

Kevin A. McTaggart

Approved by

Neil Pegg

Head, Warship Performance

Approved for release by

Kirk Foster

DRP Chair

Abstract

This report describes the prediction of appendage and viscous forces in DRDC Atlantic's ShipMo3D library for ship motions in waves. Previously, the ShipMo3D library considered only hull forces due to potential flow. Inclusion of appendage and viscous forces is essential for accurate prediction of ship sway, roll, and yaw motions. Appendage forces are caused by added mass, lift, and viscous effects. Hull viscous forces are also important and are included in the present treatment. This report introduces a method for including appendages in hull radiation and diffraction computations by representing appendages using dipole panels. Computations for a naval destroyer have indicated that inclusion of appendages in hull radiation and diffraction computations has a negligible effect on predicted motions; thus, hull and appendage forces can be evaluated separately without affecting accuracy of motion predictions. Comparisons of predictions with experiments for a steered warship model in regular waves show good agreement. Future work will incorporate hull lift forces in ship motion predictions.

Résumé

Le présent rapport décrit la prédiction des forces exercées sur les appendices et des forces de viscosité dans la bibliothèque ShipMo3D des mouvements des navires dans les vagues de RDDC Atlantique. Auparavant, la bibliothèque ShipMo3D tenait compte uniquement des forces exercées sur la coque par l'écoulement potentiel. L'inclusion des forces exercées sur les appendices et des forces de viscosité est essentielle pour prédire avec précision les mouvements de déplacement latéral, de roulis et d'embardée des navires. Les forces exercées sur les appendices sont causées par la masse ajoutée, la portance et les effets de viscosité. Les forces de viscosité de la coque sont aussi importantes et sont inclues dans les présentes opérations. Le présent rapport traite d'une méthode pour inclure les appendices dans les calculs de radiation et de diffraction de la coque en représentant les appendices au moyen de panneaux de doublets. Les calculs effectués pour un destroyer indiquent que l'inclusion des appendices dans les calculs de radiation et de diffraction de la coque a très peu d'effet sur les mouvements prévus ; les forces exercées sur la coque et les appendices peuvent donc être évaluées séparément sans que cela influe sur la précision des prédictions de mouvements. Les comparaisons entre les prédictions et les expériences avec un modèle de navire de guerre sous manœuvre dans des vagues régulières donnent une bonne concordance. Des travaux futurs incluront les forces de portance de la coque dans les prédictions des mouvements des navires.

This page intentionally left blank.

Executive summary

Introduction

DRDC Atlantic is developing a new object-oriented library for simulation of ship motions in waves. It is widely known that appendage and viscous forces significantly influence ship motions in sway, roll, and yaw. This report describes the implementation of appendage and viscous forces in the ShipMo3D library.

Principal Results

Appendage and viscous forces have been implemented in the ShipMo3D library for computations in both the frequency domain and time domain. This report introduces a method for including appendages in hull radiation and diffraction computations by representing appendages using dipole panels. Computations for a naval destroyer have indicated that inclusion of appendages in hull radiation and diffraction computations has a negligible effect on predicted motions; thus, hull and appendage forces can be evaluated separately without affecting accuracy of motion predictions. Comparisons of predictions with experiments for a steered warship model in regular waves show good agreement. Excellent agreement between frequency domain and time domain predictions indicates consistent implementation of appendage and viscous force terms.

Significance of Results

The ShipMo3D library can now model motions in waves for six degrees of freedom for a ship with steady speed and heading. Validation to date suggests that the library can be used with confidence for ships in moderate sea conditions.

Future Plans

The ShipMo3D library is being extended to model motions of a freely maneuvering ship in waves. Hull lift forces will be incorporated in future ship motion predictions.

Kevin McTaggart; 2004; Appendage and Viscous Forces for Ship Motions in Waves; DRDC Atlantic TM 2004-227; Defence R&D Canada – Atlantic.

Sommaire

Introduction

RDDC Atlantique travaille à la mise au point d'une nouvelle bibliothèque orientée objets pour la simulation des mouvements des navires dans les vagues. Il est reconnu que les forces exercées sur les appendices et les forces de viscosité influent de manière significative sur les mouvements des navires dans les situations de déplacement latéral, de roulis et d'embardée. Le présent rapport traite de l'implémentation de données sur les forces exercées sur les appendices et les forces de viscosité dans la bibliothèque ShipMo3D.

Résultats principaux

Des données sur les forces exercées sur les appendices et les forces de viscosité ont été implémentées dans la bibliothèque ShipMo3D pour effectuer des calculs dans le domaine des fréquences et le domaine temporel. Le présent rapport traite d'une méthode pour inclure les appendices dans les calculs de radiation et de diffraction de la coque en représentant les appendices au moyen de panneaux de doublets. Les calculs effectués pour un destroyer indiquent que l'inclusion des appendices dans les calculs de radiation et de diffraction de la coque a très peu d'effet sur les mouvements prévus ; les forces exercées sur la coque et les appendices peuvent donc être évaluées séparément sans que cela influe sur la précision des prédictions de mouvements. Les comparaisons entre les prédictions et les expériences avec un modèle de navire de guerre sous manœuvre dans des vagues régulières donnent une bonne concordance.

Importance des résultats

La bibliothèque ShipMo3D peut maintenant modéliser des mouvements dans les vagues sur six degrés de liberté pour un navire avec une vitesse et un cap constants. Jusqu'à maintenant, la validation laisse supposer que la bibliothèque peut être utilisée pour les navires dans des conditions de mer agitée.

Travaux ultérieurs prévus

La bibliothèque ShipMo3D enrichie permet de modéliser les mouvements d'un navire en libre manœuvre dans les vagues. Les forces de portance de la coque seront incorporées dans des prédictions futures des mouvements des navires.

Table of contents

List of tables

List of figures

1 Introduction

DRDC Atlantic is developing software components for modelling and simulation of ships in waves. Work completed to date includes predictions of forces and motions in waves for an unappended ship hull in the frequency domain [1] and time domain [2], and modelling of seaways for prediction of ship motions [3]. This report describes the inclusion of appendage and viscous forces in the ShipMo3D library.

Appendage and viscous forces must be considered for accurate prediction of ship motions in sway, roll, and yaw. Schmitke [4] was among the first to include appendage and viscous forces in ship motion predictions. The accurate prediction of viscous roll damping continues to be a challenge. Himeno [5] provides a very good overview of viscous forces influencing roll damping. These two references provide a significant foundation for incorporating appendage and viscous forces in the ShipMo3D library. The ShipMo3D library introduces a new capability for including appendages in hull radiation and diffraction computations, as discussed by McTaggart and Stredulinsky [6].

Section 2 of this report describes the axis system used for computing forces on a ship hull and appendages. Section 3 describes the prediction of forces on ship appendages, followed by the prediction of hull viscous forces in Section 4. The inclusion of appendages in hull radiation and diffraction computations is described in Section 5. Section 6 covers the modelling of a simple autopilot, which is important for simulating lateral plane motions in waves. Section 7 describes the numerical implementation of the present work, which has been validated using experimental data for a steered warship model in Section 8. Recommendations for future work are given in Section 9, followed by final conclusions in Section 10.

2 Translating Earth Axis System for Computing Forces on a Hull and Appendages

As was done in previous work on the ShipMo3D library [1, 2, 3], the present report uses a translating earth axis system that moves with the mean steady ship speed. Figure 1 shows the translating coordinate system. The relative sea direction β uses the convention shown in Figure 2, with $\beta = 180°$ representing head seas.

Note that the translating earth axis system in the present work differs from the stability-based axis system used by Schmitke [4] for deriving forces on a ship and its appendages. The stability-based axis system rotates with the instantaneous yaw

motion of the ship; thus, yaw displacement and forces dependent on yaw displacement are always zero when using a stability-based axis system. In contrast, forces in a translating earth axis system include terms proportional to yaw displacement, such as lift stiffness terms due to the angle of attack caused by yaw displacement.

3 Forces on Appendages

Forces on appendages significantly influence lateral plane motions of ships. Much of the present work is based on Schmitke [4]. In this section, radiation and diffraction forces due to appendages are assumed to be negligible. Computations by McTaggart and Stredulinsky [6] for HMCS NIPIGON confirmed that radiation and diffraction forces on appendages will have negligible influence on predicted motions for naval destroyers. The evaluation of radiation and diffraction forces on appendages is discussed in Section 5 of this report.

3.1 Foils with Small Chord Lengths - Rudders, Propeller Shaft Brackets, and Stabilizer Fins

Appendages such as rudders, propeller shaft brackets, and stabilizer fins are assumed to have small chord lengths. Figures 3 and 4 give characteristic dimensions for foils with small chord lengths.

For predicting ship motions in waves, a foil chord is considered to be small if it is small relative to both the length of the ship and to incident wavelengths. The assumption of a small chord length leads to the following:

- lift forces acting on the foil motion act at distance $\bar{c}/4$ forward of the foil centroid, where $\bar{c}$ is the mean chord length,

- lift forces due to foil motion are based on the motion at distance $\bar{c}/4$ aft of the foil centroid,

- forces due to foil added mass are based on the acceleration of the foil centroid,

- forces due to foil added mass act at the foil centroid.

The added mass of a foil moving perpendicular to its plane is follows:

$$A_p^{foil} \;=\; \rho \, \frac{\pi}{4} \, s \, \bar{c}^2 \tag{1}$$
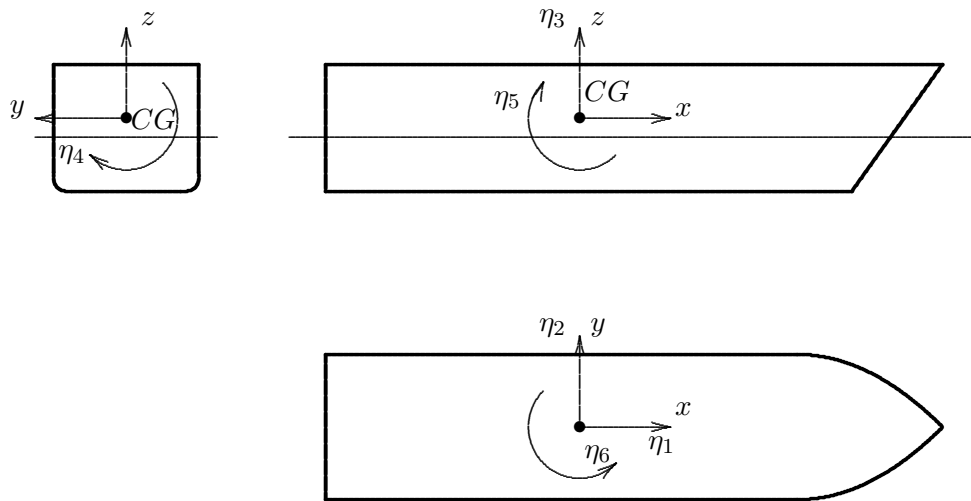
Figure 1: *Translating Earth Coordinate System*
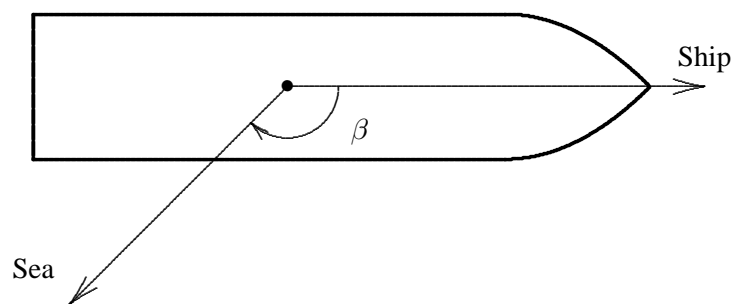
Figure 2: *Sea Direction Relative to Ship*
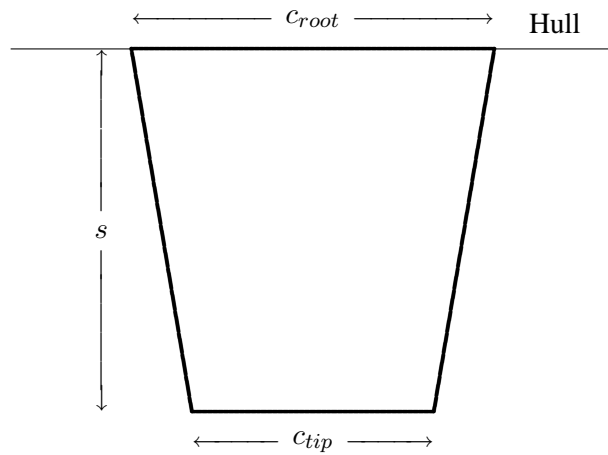
Figure 3: *Dimensions for Foil Appendage from Viewpoint Perpendicular to Foil*
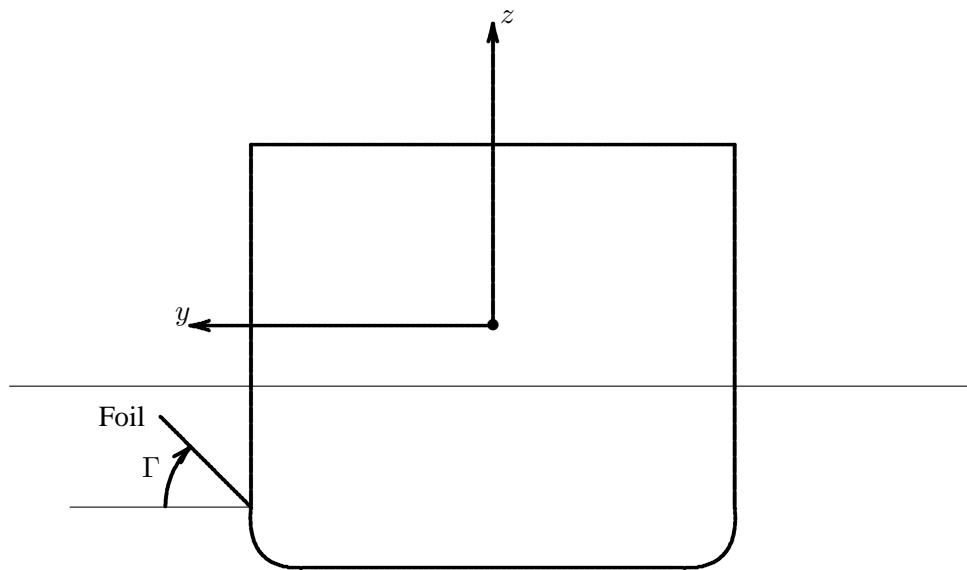
Figure 4: *Foil Dihedral Angle, View from Stern*

where ρ is water density. The lift force acting on a foil with flow velocity V at incident angle α is evaluated by:

$$F_{lift}^{foil} \;\; = \;\; \frac{1}{2}\,\rho\,S\,V^2\,\alpha\,\frac{\partial C^{lift}}{\partial \alpha} \tag{2}$$

where S is the foil area and $\partial C^{lift}/\partial \alpha$ is the lift curve slope. Equation (2) excludes a circulation delay function from Schmitke [4]. The circulation delay function is not included in the ShipMo3D library because its value is typically close to one and because it is difficult to include it consistently in frequency domain and time domain formulations. For lift forces acting on a ship foil, the following relationship is used for evaluating the incident flow speed and angle:

$$V^2\,\alpha \;\; = \;\; U\,\left(1\,+\,\frac{\Delta U^{foil}}{U}\right)\,V_p \tag{3}$$

where U is ship forward speed, ΔU^{foil} is the local velocity correction at the foil, and V_p is flow velocity perpendicular to the foil.

The lift curve slope in uniform flow can be evaluated using the following equation from Whicker and Fehlner [7]:

$$\frac{\partial C^{lift}}{\partial \alpha} \;\; = \;\; \frac{0.9 \times 4\pi\; s/\overline{c}}{1.8 + \sqrt{\left(2s/\overline{c}\right)^2 + 4.0}} \tag{4}$$

Figure 5 shows the variation of lift coefficient slope with aspect ratio using the above equation, and also the lift coefficient slope based on low aspect ratio theory as follows:

$$\frac{\partial C^{lift}}{\partial \alpha} \;\; = \;\; \pi\; s/\overline{c} \tag{5}$$

Using the terms given above, the lift damping due to a foil moving with velocity perpendicular to its plane can be expressed as:

$$B_p^{foil} \;\; = \;\; \frac{1}{2}\,\rho\,U\,\left(1\,+\,\frac{\Delta U^{foil}}{U}\right)\,S\,\frac{\partial C^{lift}}{\partial \alpha} \tag{6}$$

The local incident velocity ratio $\left(1\,+\,\Delta U^{foil}/U\right)$ will often be less than 1.0 due to the influence of the hull boundary layer. Propeller-induced flow and the influence of the hull on the incident potential flow will also influence the velocity increment ΔU^{foil}. SHIPMO7 [8] includes the effect of the hull boundary layer when evaluating local incident flow velocity. The turbulent boundary layer can be modelled
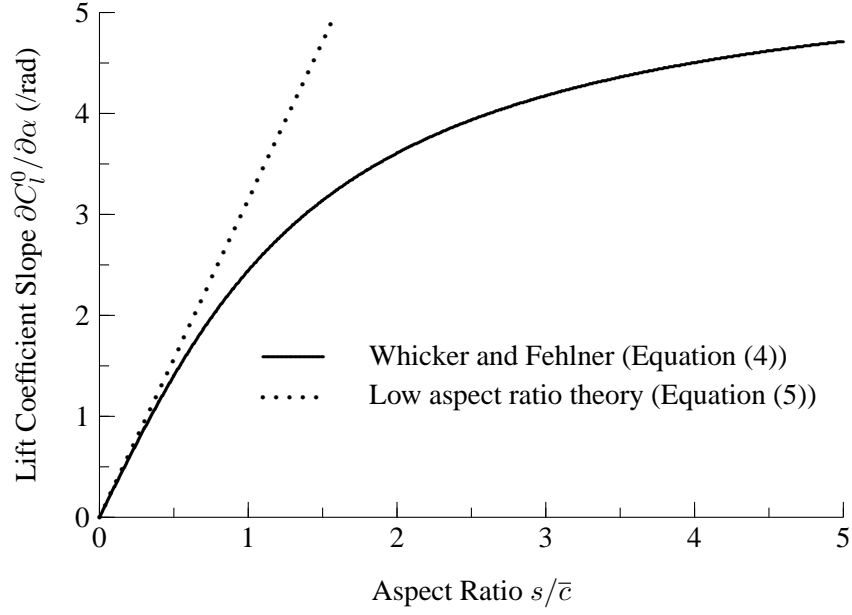
Figure 5: *Foil Lift Coefficient Slope*

using a one-seventh power approximation [9], with the boundary layer thickness given by:

$$\delta_b \quad = \quad \frac{0.377 \left(x_{FP} - x^{foil} \right)}{\left(Re^{foil} \right)^{0.2}} \tag{7}$$

The foil Reynolds number is dependent on the distance of the foil from the hull forward perpendicular as follows:

$$Re^{foil} \quad = \quad \frac{U \left(x_{FP} - x^{foil} \right)}{\nu} \tag{8}$$

where x_{FP} is the longitudinal location of the forward perpendicular, x_{foil} is the longitudinal location of the foil, and ν is the kinematic viscosity of water. The speed correction factor to account for the influence of the hull boundary layer is given by:

$$\left(1 + \Delta U^{foil}/U \right) \quad = \quad 1 + \frac{\delta_b}{2sc_{root}} \left[\frac{\delta_b \left(c_{root} - c_{tip} \right)}{8s} - \frac{4\, c_{root}}{9} \right] \tag{9}$$

Figure 6 shows the influence of the hull boundary layer on lift of rectangular foils near the stern of a frigate. As ship speed increases, the boundary layer thickness and corresponding speed reduction decrease. As foil span increases, the relative importance of the boundary layer decreases.
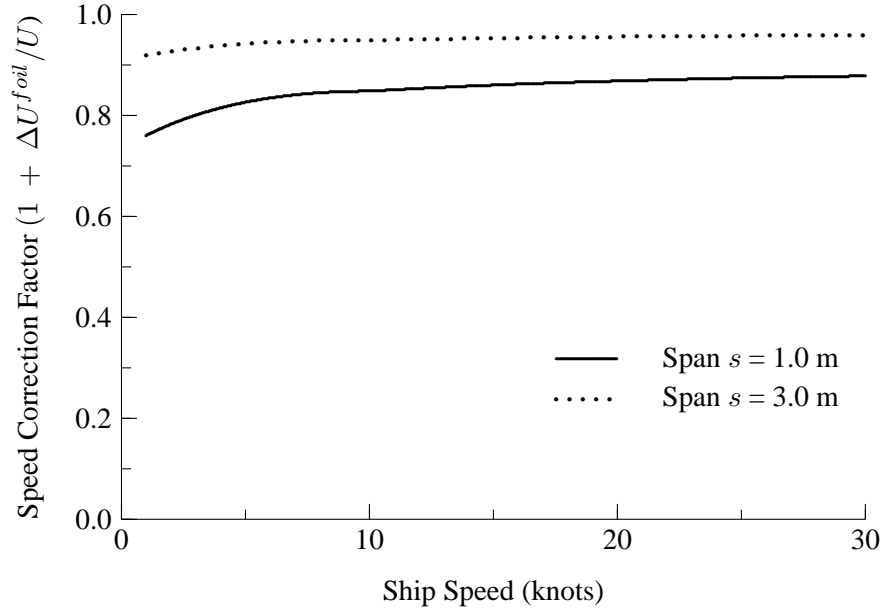
Figure 6: *Influence of Hull Boundary Layer on Lift Forces from Rectangular Foils Near Stern of Frigate - 100 m aft of Fore Perpendicular*

For roll motions, ship damping forces due to potential flow are often small and viscous forces can be significant. Viscous forces on foils are evaluated by treating them as flat plates oriented at angles of high incidence to flow, with drag forces as follows:

$$F^{foil-visc} \quad = \quad \frac{1}{2} \, \rho \, V_p^2 \, s \, \overline{c} \, C_d \tag{10}$$

where C_d is the drag coefficient, which is assumed to be 1.17 for a flat plate.

Using the forces described above, hydrodynamic coefficients for foils appended to ships can be evaluated. Each foil has a dihedral angle Γ relative to the y axis as shown in Figure 4. Each foil has an effective roll radius for lift forces based on the location of its centroid given as follows:

$$r_l \quad = \quad \overline{y} \cos \Gamma \, + \, \overline{z} \sin \Gamma \tag{11}$$

For roll-roll added mass and damping, the nominal square value of the effective roll radius is required, and is evaluated as follows:

$$\widetilde{r_l^2} \quad = \quad \frac{1}{S} \int_S (y \cos \Gamma \, + \, z \sin \Gamma)^2 \, dS \tag{12}$$

The resulting hydrodynamic coefficients in translating earth axes are:

$$A_{22}^{foil} \quad = \quad A_p^{foil} \, \sin^2 \Gamma \tag{13}$$

$$B_{22}^{foil} = B_p^{foil} \sin^2 \Gamma \tag{14}$$

$$A_{23}^{foil} = -A_p^{foil} \cos \Gamma \sin \Gamma \tag{15}$$

$$B_{23}^{foil} = -B_p^{foil} \cos \Gamma \sin \Gamma \tag{16}$$

$$A_{24}^{foil} = -A_p^{foil} \sin \Gamma \, r_l \tag{17}$$

$$B_{24}^{foil} = -B_p^{foil} \sin \Gamma \, r_l \tag{18}$$

$$A_{25}^{foil} = -\overline{x} A_{23}^{foil} \tag{19}$$

$$B_{25}^{foil} = -(\overline{x} - \overline{c}/4) \, B_{23}^{foil} \tag{20}$$

$$C_{25}^{foil} = U \, B_{23}^{foil} \tag{21}$$

$$A_{26}^{foil} = \overline{x} \, A_{22}^{foil} \tag{22}$$

$$B_{26}^{foil} = (\overline{x} - \overline{c}/4) \, B_{22}^{foil} \tag{23}$$

$$C_{26}^{foil} = -U \, B_{22}^{foil} \tag{24}$$

$$A_{32}^{foil} = -A_p^{foil} \cos \Gamma \sin \Gamma \tag{25}$$

$$B_{32}^{foil} = -B_p^{foil} \cos \Gamma \sin \Gamma \tag{26}$$

$$A_{33}^{foil} = A_p^{foil} \cos^2 \Gamma \tag{27}$$

$$B_{33}^{foil} = B_p^{foil} \cos^2 \Gamma \tag{28}$$

$$A_{34}^{foil} = A_p^{foil} \cos \Gamma \, r_l \tag{29}$$

$$B_{34}^{foil} = B_p^{foil} \cos \Gamma \, r_l \tag{30}$$

$$A_{35}^{foil} = -\overline{x} \, A_{33}^{foil} \tag{31}$$

$$B_{35}^{foil} = -(\overline{x} - \overline{c}/4) \, B_{33}^{foil} \tag{32}$$

$$C_{35}^{foil} = U \, B_{33}^{foil} \tag{33}$$

$$A_{36}^{foil} = \overline{x} \, A_{32}^{foil} \tag{34}$$

$$B_{36}^{foil} = (\overline{x} - \overline{c}/4) \, B_{32}^{foil} \tag{35}$$

$$C_{36}^{foil} = -U \, B_{32}^{foil} \tag{36}$$

$$A_{42}^{foil} = -A_p^{foil} \sin \Gamma \, r_l \tag{37}$$

$$B_{42}^{foil} = -B_p^{foil} \sin \Gamma \, r_l \tag{38}$$

$$A_{43}^{foil} = A_p^{foil} \cos \Gamma \, r_l \tag{39}$$

$$B_{43}^{foil} = B_p^{foil} \cos \Gamma \, r_l \tag{40}$$

$$A_{44}^{foil} = A_p^{foil} \, \widetilde{r_l^2} \tag{41}$$

$$B_{44}^{foil} = B_p^{foil} \, \widetilde{r_l^2} \, + \, B_{44}^{foil-v} \tag{42}$$

$$A_{45}^{foil} = -\overline{x} \, A_{43}^{foil} \tag{43}$$

$$B_{45}^{foil} = -(\overline{x} - \overline{c}/4) \, B_{43}^{foil} \tag{44}$$

$$C_{45}^{foil} = U \, B_{43}^{foil} \tag{45}$$

$$A_{46}^{foil} = \overline{x}\, A_{42}^{foil} \tag{46}$$

$$B_{46}^{foil} = (\overline{x} - \overline{c}/4)\, B_{42}^{foil} \tag{47}$$

$$C_{46}^{foil} = -U\, B_{42}^{foil} \tag{48}$$

$$A_{62}^{foil} = \overline{x}\, A_{22}^{foil} \tag{49}$$

$$B_{62}^{foil} = (\overline{x} + \overline{c}/2)\, B_{22}^{foil} \tag{50}$$

$$A_{63}^{foil} = \overline{x}\, A_{23}^{foil} \tag{51}$$

$$B_{63}^{foil} = (\overline{x} + \overline{c}/2)\, B_{23}^{foil} \tag{52}$$

$$A_{64}^{foil} = \overline{x}\, A_{24}^{foil} \tag{53}$$

$$B_{64}^{foil} = (\overline{x} + \overline{c}/2)\, B_{24}^{foil} \tag{54}$$

$$A_{65}^{foil} = -\overline{x}^2\, A_{23}^{foil} \tag{55}$$

$$B_{65}^{foil} = -(\overline{x} + \overline{c}/2)\, (\overline{x} + \overline{c}/2)\, B_{23}^{foil} \tag{56}$$

$$C_{65}^{foil} = U\, B_{63}^{foil} \tag{57}$$

$$A_{66}^{foil} = \overline{x}^2\, A_{22}^{foil} \tag{58}$$

$$B_{66}^{foil} = (\overline{x} - \overline{c}/4)\, (\overline{x} + \overline{c}/4)\, B_{22}^{foil} \tag{59}$$

$$C_{66}^{foil} = -U\, B_{62}^{foil} \tag{60}$$

The roll damping term B_{44}^{foil} includes a contribution $B_{44}^{foil-visc}$ from viscous damping which can be evaluated based on Equation (10). The viscous roll moment induced by roll velocity $\dot{\eta}_4$ will be:

$$F_4^{foil-visc} = \frac{1}{2}\, \rho\, \dot{\eta}_4^2\, S\, C_d\, \widetilde{r_v^3} \tag{61}$$

where $\widetilde{r_v^3}$ is the effective cube of the roll moment arm for viscous forces given by:

$$\widetilde{r_v^3} = \frac{1}{S} \int_S (y\,\cos\Gamma + z\,\sin\Gamma)^2 \sqrt{y^2 + z^2}\, dS \tag{62}$$

For computations in the time domain, the viscous roll damping coefficient is:

$$B_{44}^{foil-visc} = \frac{1}{2}\, \rho\, \dot{\eta}_4\, S\, C_d\, \widetilde{r_v^3} \tag{63}$$

For computations in the frequency domain, the equivalent linear damping coefficient based on energy dissipation is:

$$B_{44}^{foil-visc} = \frac{4}{3\pi}\, \rho\, \omega_e\, \hat{\eta}_4\, \widetilde{r_v^3}\, S\, C_d \tag{64}$$

where $\hat{\eta}_4$ is the roll amplitude.

When foils are in the presence of waves, excitation forces will occur due to added mass and lift in the presence of incident flow. The excitation forces can be computed using the added mass and damping terms previously computed:

$$F_j^{foil} = a_y\, A_{j2}^{foil} + a_z\, A_{j3}^{foil} + u_y\, B_{j2}^{foil} + u_z\, B_{j3}^{foil} \tag{65}$$

where a_y and a_z are the horizontal and vertical wave-induced flow accelerations, and u_y and u_z are the horizontal and vertical wave-induced flow velocities.

Some foils such as rudders and stabilizing fins will have deflections which will induce forces on the ship. Schmitke [10] presents forces arising from rudders and stabilizing fins. In the current work, forces proportional to deflection acceleration and velocity are assumed to be negligible. The convention used for foil deflection is positive for counter-clockwise when viewed from inside the ship. For example, a conventional vertical rudder will have a positive deflection angle if it is counter-clockwise when viewed from above. The lift force acting perpendicular to a rudder due to its deflection δ^{rudder} will be:

$$F_{lift}^{rudder} \;\; = \;\; \frac{1}{2} \, \rho \, S \, V^2 \; \frac{\partial C^{lift}}{\partial \alpha} \; \delta^{rudder} \tag{66}$$

The stiffness coefficient for the rudder deflection can be expressed as:

$$C_{\delta}^{rudder} \;\; = \;\; \frac{1}{2} \, \rho \, S \, U^2 \; \left(1 \, + \, \frac{\Delta U^{foil}}{U} \right)^2 \; \frac{\partial C^{lift}}{\partial \alpha} \tag{67}$$

Stiffness coefficients relating ship forces to rudder deflections are:

$$C_{2\delta}^{rudder} \;\; = \;\; C_{\delta}^{rudder} \; \sin \Gamma \tag{68}$$

$$C_{3\delta}^{rudder} \;\; = \;\; -C_{\delta}^{rudder} \; \cos \Gamma \tag{69}$$

$$C_{4\delta}^{rudder} \;\; = \;\; -C_{\delta}^{rudder} \; r_l \tag{70}$$

$$C_{5\delta}^{rudder} \;\; = \;\; -C_{\delta}^{3} \; (\overline{x} \, + \, \overline{c}/2) \tag{71}$$

$$C_{6\delta}^{rudder} \;\; = \;\; C_{2\delta}^{rudder} \; (\overline{x} \, + \, \overline{c}/2) \tag{72}$$

3.2   Bilge Keels and Other Foils with Long Chord Lengths and Low Aspect Ratios

So far discussion has been limited to foils with small chord lengths. In contrast, bilge keels have long chord lengths, which are non-negligible relative to the length of the ship and incident wavelengths. Bilge keels are assumed to have low aspect ratios with lift curve slope given by Equation (5). Figure 5 suggests that the assumption of low aspect ratio is valid for aspect ratios less than 0.3, which is consistent with typical bilge keels. The present discussion is also applicable to skegs and other appendages with long chord lengths and low aspect ratios.

The added mass of a bilge keel moving perpendicular to its plane is determined from the following equation based on potential flow theory for a flat plate [11]:

$$A_p^{bk} \;\; = \;\; \rho \, \frac{\pi}{2} \, \int_{x_{aft}}^{x_{fore}} s^2(x) dx \tag{73}$$

where x_{aft} is the aft extent of the bilge keel, x_{fore} is the forward extent of the bilge keel, and $s(x)$ is the local span.

Newman [9] and Crane, Eda, and Landsburg [12] discuss lift forces on low aspect ratio foils. Equation (5) indicates that the lift coefficient slope of a low aspect foil is proportional to the aspect ratio. Consequently, the lift force acting on a bilge keel will be independent of chord length, and can be expressed as:

$$F_{lift}^{bk} \;=\; \frac{1}{2} \, \rho \, s_{max}^2 \, V^2 \, \alpha \, \pi \tag{74}$$

If the bilge keel has constant span (i.e., independent of x), then the lift force will be concentrated at the leading edge. Note that the lift magnitude and effective location will be unaffected if local span decreases downstream of the location of maximum span. To simplify the analysis of lift forces on bilge keels, the lift force is evaluated at the foremost location at which the maximum span occurs, denoted x_{lift}.

The lift damping due to a bilge keel moving perpendicular to its plane can be expressed as:

$$B_p^{bk} \;=\; \frac{1}{2} \, \rho \, U \, \left(1 \,+\, \Delta U^{bk}/U\right) \, s_{max}^2 \, \pi \tag{75}$$

where ΔU^{bk} is the local incident velocity correction at the bilge keel.

Viscous eddy damping from bilge keels can be a significant fraction of total roll damping, particularly at low ship speeds. The viscous drag force on a bilge keel can be expressed as follows:

$$F^{bk-visc} \;=\; \frac{1}{2} \, \rho \, C_d \int_{x_{aft}} x_{fore} \, V_p^2(x) \, s^2(x) \, dx \tag{76}$$

Forces acting on bilge keels are significantly influenced by two flow phenomena that are typically neglected for shorter foils of larger aspect ratios. Drag coefficients for oscillating bilge keels are often much greater than the value of 1.17 for a flat plate in uniform flow. The higher drag coefficients are due to the oscillating nature of the flow, and increase with decreasing ratio of foil span to motion amplitude. The second phenomenon that should be considered is the influence of the hull on the incident flow normal to the bilge keel and resulting drag. This effect can be modelled using a local roll velocity ratio v, which is the ratio of the local normal velocity induced by roll to the velocity in the absence of the hull.

Using the forces described above, hydrodynamic coefficients for bilge keels can be evaluated. The local span of a bilge keel is assumed to be small relative to the distance from the ship center of gravity; thus, the effective y and z locations are

taken at mid-span of the bilge keel. The resulting hydrodynamic coefficients in translating earth axes are:

$$A_{22}^{bk} = \rho \, \frac{\pi}{2} \int_{x_{aft}}^{x_{fore}} s^2(x) \, \sin^2 \Gamma(x) \, dx \tag{77}$$

$$B_{22}^{bk} = B_p^{bk} \, \sin^2 \Gamma(x_{lift}) \tag{78}$$

$$A_{23}^{bk} = -\rho \, \frac{\pi}{2} \int_{x_{aft}}^{x_{fore}} s^2(x) \, \sin \Gamma(x) \, \cos \Gamma(x) \, dx \tag{79}$$

$$B_{23}^{bk} = -B_p^{bk} \, \sin \Gamma(x_{lift}) \, \cos \Gamma(x_{lift}) \tag{80}$$

$$A_{24}^{bk} = -\rho \, \frac{\pi}{2} \int_{x_{aft}}^{x_{fore}} s^2(x) \, \sin \Gamma(x) \, r_l(x) \, dx \tag{81}$$

$$B_{24}^{bk} = -B_p^{bk} \, \sin \Gamma(x_{lift}) \, r_l(x_{lift}) \tag{82}$$

$$A_{25}^{bk} = \rho \, \frac{\pi}{2} \int_{x_{aft}}^{x_{fore}} s^2(x) \, x \, \sin \Gamma(x) \, \cos \Gamma(x) \, dx \tag{83}$$

$$B_{25}^{bk} = B_p^{bk} \, x \, \sin \Gamma(x_{lift}) \, \cos \Gamma(x_{lift}) \tag{84}$$

$$C_{25}^{bk} = U \, B_{23}^{bk} \tag{85}$$

$$A_{26}^{bk} = \rho \, \frac{\pi}{2} \int_{x_{aft}}^{x_{fore}} s^2(x) \, \sin^2 \Gamma(x) \, x \, dx \tag{86}$$

$$B_{26}^{bk} = x_{lift} \, B_{22}^{bk} \tag{87}$$

$$C_{26}^{bk} = -U \, B_{22}^{bk} \tag{88}$$

$$A_{32}^{bk} = -\rho \, \frac{\pi}{2} \int_{x_{aft}}^{x_{fore}} s^2(x) \, \sin \Gamma(x) \, \cos \Gamma(x) \, dx \tag{89}$$

$$B_{32}^{bk} = -B_p^{bk} \, \sin \Gamma(x_{lift}) \, \cos \Gamma(x_{lift}) \tag{90}$$

$$A_{33}^{bk} = \rho \, \frac{\pi}{2} \int_{x_{aft}}^{x_{fore}} s^2(x) \, \cos^2 \Gamma(x) \, dx \tag{91}$$

$$B_{33}^{bk} = B_p^{bk} \, \cos^2 \Gamma(x_{lift}) \tag{92}$$

$$A_{34}^{bk} = \rho \, \frac{\pi}{2} \int_{x_{aft}}^{x_{fore}} s^2(x) \, \cos \Gamma \, r_l(x) \, dx \tag{93}$$

$$B_{34}^{bk} = B_p^{bk} \, \cos \Gamma(x_{lift}) \, r_l(x_{lift}) \tag{94}$$

$$A_{42}^{bk} = A_{24}^{foil} \tag{95}$$

$$B_{42}^{bk} = B_{24}^{bk} \tag{96}$$

$$A_{43}^{bk} = \rho \, \frac{\pi}{2} \int_{x_{aft}}^{x_{fore}} s^2(x) \, \cos \Gamma \, r_l(x) \, dx \tag{97}$$

$$B_{43}^{bk} = B_p^{bk} \, \cos \Gamma(x_{lift}) \, r_l(x_{lift}) \tag{98}$$

$$A_{44}^{bk} = \rho \, \frac{\pi}{2} \int_{x_{aft}}^{x_{fore}} s^2(x) \, r_l(x)^2 \, dx \tag{99}$$

$$B_{44}^{bk} = B_p^{bk} \ \widetilde{r_l^2}(x_{lift}) \ + \ B_{44}^{foil-visc} \tag{100}$$

$$A_{45}^{bk} = -\rho \ \frac{\pi}{2} \int_{x_{aft}}^{x_{fore}} s^2(x) \ x \ \cos\Gamma \ r_l(x) \ dx \tag{101}$$

$$B_{45}^{bk} = B_p^{bk} \ x_{lift} \ \cos\Gamma(x_{lift}) \ r_l(x_{lift}) \tag{102}$$

$$C_{45}^{bk} = U \ B_{43}^{bk} \tag{103}$$

$$A_{46}^{bk} = -\rho \ \frac{\pi}{2} \int_{x_{aft}}^{x_{fore}} s^2(x) \ \sin\Gamma(x) \ r_l(x) \ x \ dx \tag{104}$$

$$B_{46}^{bk} = x_{lift} \ B_{42}^{bk} \tag{105}$$

$$C_{46}^{bk} = -U \ B_{42}^{bk} \tag{106}$$

$$A_{62}^{bk} = \rho \ \frac{\pi}{2} \int_{x_{aft}}^{x_{fore}} s^2(x) \ \sin^2\Gamma(x) \ x \ dx \tag{107}$$

$$B_{62}^{bk} = x_{lift} \ B_{22}^{bk} \tag{108}$$

$$A_{63}^{bk} = -\rho \ \frac{\pi}{2} \int_{x_{aft}}^{x_{fore}} s^2(x) \ \sin\Gamma(x) \ \cos\Gamma(x) \ x \ dx \tag{109}$$

$$B_{63}^{bk} = x_{lift} \ B_{23}^{bk} \tag{110}$$

$$A_{64}^{bk} = -\rho \ \frac{\pi}{2} \int_{x_{aft}}^{x_{fore}} s^2(x) \ \sin\Gamma(x) \ r_l(x) \ x \ dx \tag{111}$$

$$B_{64}^{bk} = x_{lift} \ B_{24}^{bk} \tag{112}$$

$$A_{65}^{bk} = \rho \ \frac{\pi}{2} \int_{x_{aft}}^{x_{fore}} s^2(x) \ \sin\Gamma(x) \ \cos\Gamma(x) \ x^2 \ dx \tag{113}$$

$$B_{65}^{bk} = -x_{lift}^2 \ B_{23}^{bk} \tag{114}$$

$$C_{65}^{bk} = U \ B_{63}^{bk} \tag{115}$$

$$A_{66}^{bk} = \rho \ \frac{\pi}{2} \int_{x_{aft}}^{x_{fore}} s^2(x) \ \sin^2\Gamma(x) \ x^2 \ dx \tag{116}$$

$$B_{66}^{bk} = x_{lift}^2 \ B_{22}^{bk} \tag{117}$$

$$C_{66}^{bk} = -U \ B_{62}^{bk} \tag{118}$$

The effective square of the local added mass moment arm is given by:

$$\widetilde{r_l^2}(x) = [\bar{y}(x) \ \cos\Gamma(x) \ + \ \bar{z}(x) \ \sin\Gamma(x)]^2 \tag{119}$$

The roll damping term B_{44}^{bk} includes a contribution $B_{44}^{bk-visc}$ from viscous damping which can be evaluated based on Equation (76). The viscous roll moment induced by roll velocity $\dot{\eta}_4$ will be:

$$F_4^{bk-visc} = \frac{1}{2} \ \rho \ \dot{\eta}_4^2 \ \upsilon^2 \int_{x_{aft}}^{x_{fore}} s(x) \ C_d(x) \ \widetilde{r^3}(x) \ dx \tag{120}$$

where $\widetilde{r}_v^3(x)$ is the effective cube of the local roll moment arm given by:

$$\widetilde{r}_v^3(x) \;\; = \;\; [\overline{y}(x) \; \cos \Gamma(x) \; + \; z(x) \; \sin \Gamma(x)]^2 \; \sqrt{\overline{y}^2(x) \; + \overline{z}^2(x)} \quad (121)$$

For computations in the time domain, the viscous roll damping coefficient is:

$$B_{44}^{bk-visc} \;\; = \;\; \frac{1}{2} \; \rho \; \dot{\eta}_4 \; \int_{x_{aft}}^{x_{fore}} \; s(x) \; C_d(x) \; \widetilde{r}_v^3(x) \; dx \quad (122)$$

For computations in the frequency domain, the equivalent linear damping coefficient based on energy dissipation is:

$$B_{44}^{bk-visc} \;\; = \;\; \frac{4}{3\pi} \; \rho \; \omega_e \; \hat{\eta}_4 \; \int_{x_{aft}}^{x_{fore}} \; s(x) \; C_d(x) \; \widetilde{r}_v^3(x) \; dx \quad (123)$$

Excitation forces acting on bilge keels arise from both added mass and lift components, and are evaluated as follows:

$$F_j^{bk} \;\; = \;\; a_y \; A_{j2}^{bk} \; + \; a_z \; A_{j3}^{bk} \; + \; u_y \; B_{j2}^{bk} \; + \; u_z \; B_{j3}^{bk} \; \text{for } j = 2 - 6 \quad (124)$$

The flow velocity components a_y, a_z, u_y, and u_z are evaluated at the bilge keel centroid of area. For appendages which are long relative to incident wavelengths, it is recommended that that excitation forces be evaluated using several longitudinal segments.

3.3 Drag Coefficients and Roll Velocity Ratios for Bilge Keels

One of the most challenging problems in seakeeping computations is the selection of appropriate drag coefficients for bilge keels. Note that the present discussion is also applicable to other long foils of low aspect ratio, such as skegs. Roll motion predictions can be very sensitive to input drag coefficients for bilge keels. Furthermore, different prediction methods often give widely varying results for bilge keel drag coefficients. One common feature among results from different prediction methods is that the drag coefficient increases with decreasing roll amplitude. At small roll amplitudes, experimental results [5] indicate that bilge keel drag coefficients will often exceed 10, a surprising finding considering that the drag coefficient of a flat plate normal to uniform flow is approximately 1.17. The high observed drag coefficients for bilge keels are due to the oscillatory nature of the bilge keel motions, with drag coefficients generally increasing as the ratio of the bilge keel span to motion amplitude decreases.

Ikeda's method for predicting bilge keel drag coefficients [5, 13] is widely used. The drag coefficient is given by:

$$C_d = \left[22.5 \frac{s}{\pi \ r_{BK} \ \hat{\eta}_4} + 2.4 \right] \tag{125}$$

where r_{BK} is the roll radius from the ship centre of gravity to the bilge keel. Ikeda's method uses the following equation for the the local roll velocity ratio:

$$\upsilon = 1.0 + 0.3 \exp\left[-160 \left(1.0 - \frac{A_x}{B_x \ T_x} \right) \right] \tag{126}$$

where A_x is hull cross-sectional area, B_x is hull sectional beam, and T_x is hull sectional draft. Figure 7 shows the local roll velocity ratio as a function of hull sectional area coefficient.

SHIPMO7 [8] and it's predecessors use a method developed by Kato [14] and described by Schmitke [4] for computing bilge keel drag coefficients. This method appears to be overly complex given the relatively limited number of parameters upon which it is based. Using calculations for the destroyer HMCS NIPIGON from McTaggart and Stredulinsky [6], the following simplified equations can be developed from Kato's method:

$$C_d = 5 \left(\frac{r_{BK} \ \widehat{\dot{\eta}}_4}{\sqrt{g \ s}} \right)^{-0.6} \tag{127}$$

$$\upsilon = \sqrt{1.0 + 3.5 \exp\left(\frac{-11 R_{bilge}}{r_{BK}} \right)} \tag{128}$$

where R_{bilge} is the hull bilge radius. In contrast to Ikeda's method, Kato's equation for drag coefficient has a roll velocity amplitude term $\widehat{\dot{\eta}}_4$ instead of a roll amplitude term $\widehat{\eta}_4$. Furthermore, Kato's method includes gravitational acceleration g. Due to the submergence of typical bilge keels and resulting lack of radiated waves, it is questionable whether gravitational acceleration actually influences their viscous roll damping. However, good roll predictions for HMCS NIPIGON [6, 15] obtained using Kato's formulation suggest that the approach has merit. Given that Kato's method gives good results for HMCS NIPIGON, with bilge keel parameters given in Table 1, the following new equation is proposed for the drag coefficient dependent on roll amplitude rather than roll velocity amplitude:

$$C_d = 16 \left(\frac{r_{BK} \ \widehat{\eta}_4}{s} \right)^{-0.6} \tag{129}$$

It should be emphasized that Equations (127) and (129) are initial attempts at simplified approaches based on Kato's method. Ideally, numerical values in Equations

Table 1: *Bilge Keel Parameters for HMCS Nipigon*

Length c	26.5 m
Span s	0.61 m
Average bilge keel radius $\overline{r}_{BK}$	6.8 m
Average bilge hull radius $\overline{R}_{bilge}$	3.2 m
Ship natural roll period	10.6 s

(127) and (129) should be optimized based on analysis of large volumes of experimental data.

To compare local roll velocity ratios from Ikeda's and Kato's methods, it is useful to consider rectangular hull sections with rounded corners. The cross-sectional area is given by the following:

$$A_x \;=\; B_x\,T_x \;-\; \left(2 \,-\, \frac{\pi}{2}\right)\,R_{bilge}^2 \tag{130}$$

Figures 7 and 8 show local roll velocity ratios as functions of sectional area coefficient and nondimensional bilge radius for rounded rectangular sections with a beam B_x of 8 m, a draft T_x of 4 m, and the center of gravity located 1 m above the waterline. Bilge keel radii r_{BK} are evaluated at the mid-span location for bilge keels with spans of 0.6 m. For sections with less rounded corners (i.e., larger area coefficients and smaller non-dimensional bilge radii), local roll velocity ratios from Kato's method are much greater than those from Ikeda's method. Fortunately, the influence of differences between the two methods is mitigated by the fact that bilge keel roll damping is typically of lesser relative importance for hull sections with small bilge radii.

As an alternative to the methods of Ikeda and Kato, Lloyd [16] presents plotted bilge keel drag coefficients and associated equations based on experimental data Unfortunately, Lloyd's equations appear to have errors while the plotted results appear to be correct. The following equations have been developed to represent Lloyd's plotted results:

$$C_d \;=\; 1.17 + 11.23\,a_{Cd}\left[1 \;-\; \exp\left(-\frac{2s/c)}{b_{Cd}}\right)\right] \tag{131}$$

$$a_{Cd} \;=\; 11.23\,\exp\left[-\frac{\hat{\eta}_4\,r_{BK}}{0.3\,\sqrt{s\,c}}\right] \tag{132}$$

$$b_{Cd} \;=\; 0.0125 \;+\; 0.025\,\hat{\eta}_4\,r_{BK}/\sqrt{s\,c} \tag{133}$$

For Equations (132) and (133), the roll amplitude $\hat{\eta}_4$ is given in radians.
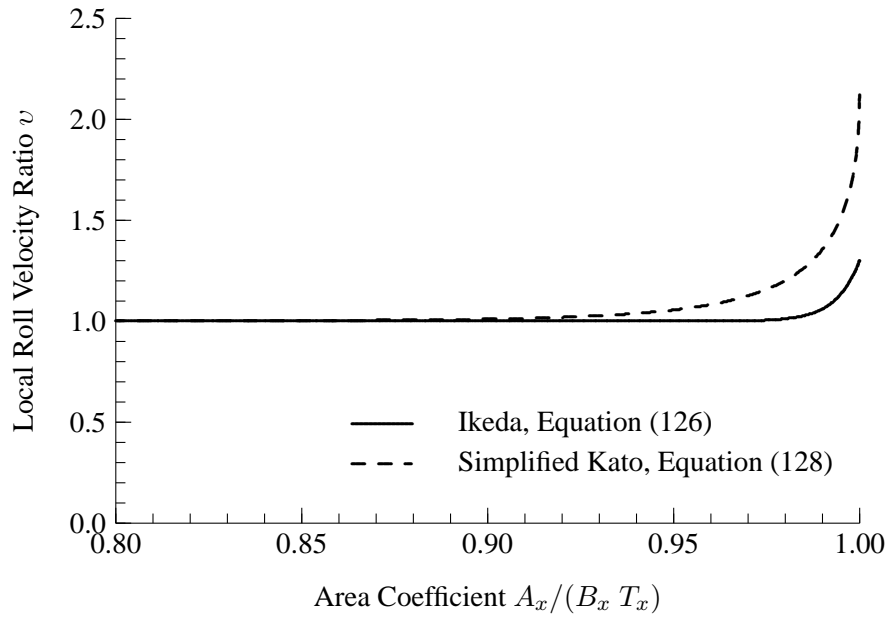
Figure 7: *Local Roll Velocity Ratio Versus Sectional Area Coefficient for Rectangular Hull Section with Rounded Corners*
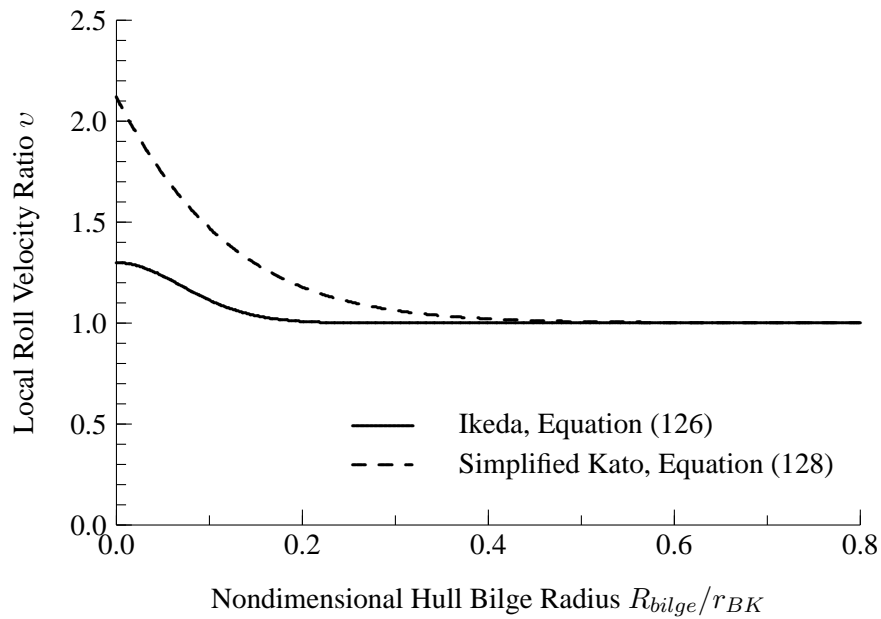
Figure 8: *Local Roll Velocity Ratio Versus Nondimensional Hull Bilge Radius for Rectangular Hull Section with Rounded Corners*
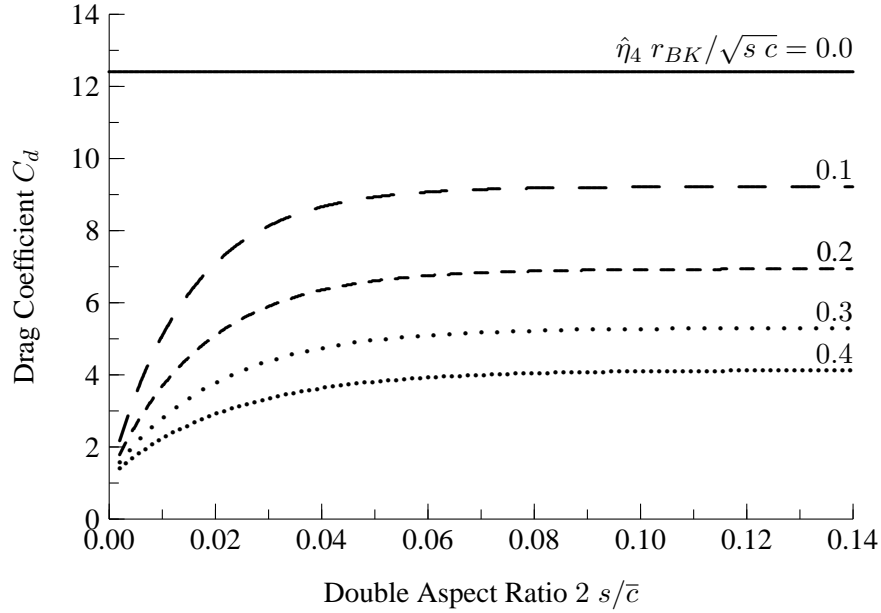
Figure 9: *Bilge Keel Drag Coefficients based on Lloyd [16]*

Figure 10 shows predicted bilge keel drag coefficients versus roll amplitude for HMCS NIPIGON. There are significant differences among the 3 different methods, particulary at low roll amplitudes for which Lloyd's method gives much smaller drag coefficients.

4 Viscous Hull Roll Damping

When a ship hull rolls in waves, significant damping forces arise from eddy making and skin friction. Schmitke [4] and Graham [17] discuss prediction of hull eddy making and skin friction forces within strip theory computations. This section presents methods for computing viscous hull roll damping for a panelled ship hull.

4.1 Formulation for Hull Eddy-Making Roll Damping

SHIPMO7 [8] and its predecessors evaluate hull eddy-making roll damping using Tanaka's method [18]. Graham [17] gives a detailed description of the SHIPMO implementation. Tanaka's method is based on empirical expressions based on sectional geometric parameters.

A new approach is introduced here for computing eddy-making roll damping using a hull geometry described by surface panels. Like Tanaka's method, the new approach correctly models the limiting cases of a circular cylindrical hull with zero
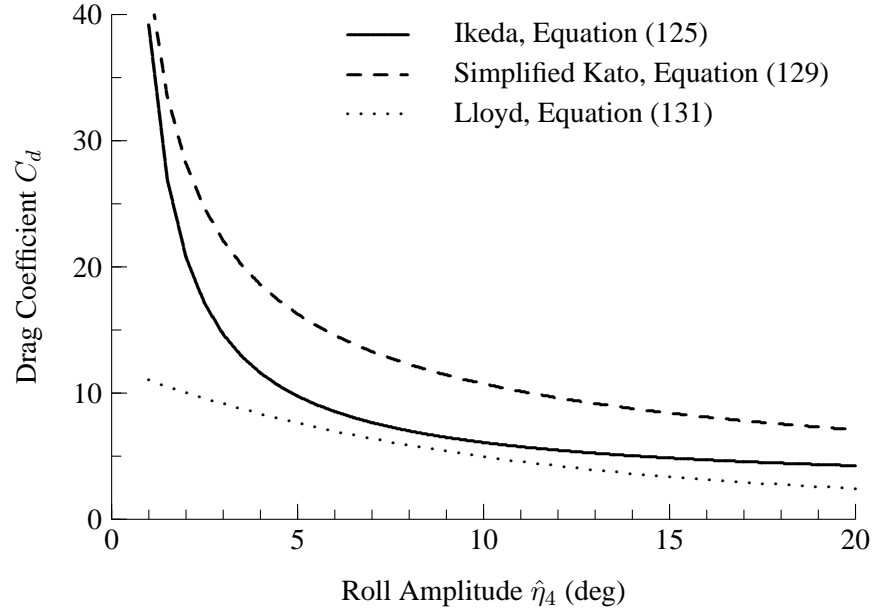
Figure 10: *Predicted Bilge Keel Drag Coefficient Versus Roll Amplitude for HMCS NIPIGON*

eddy-making damping and a hull acting as a flat plate. Using a flat plate analogy, the eddy-making damping moment at zero ship speed is given by:

$$F_4^{hull-eddy} = \frac{1}{2} \rho \, |\dot{\eta}_4| \, \dot{\eta}_4 \, C_{eddy}^{hull} \, \frac{1}{2} \int_{S_{hull}} n_4^2 \, \sqrt{y^2 + z^2} \, dS \qquad (134)$$

where C_{eddy}^{hull} is the hull drag force coefficient and n_4 is the local roll normal given by:

$$n_4 = y \, n_z - z \, n_y \qquad (135)$$

As a first approximation, the drag coefficient C_{eddy}^{hull} can be given a value of 1.17 based on a flat plate moving normal to flow. The fraction of 1/2 preceeding the integral in Equation (134) accounts for the integral including both the starboard and port sides of the hull.

For computations in the time domain, the hull eddy-making roll damping coefficient can be developed from Equation (134). Ikeda et al. [19] indicate that hull eddy-making damping decreases significantly with forward ship speed, and have developed the following relationship:

$$\frac{B_{44}^{hull-eddy}(U)}{B_{44}^{hull-eddy}(0)} = \frac{1}{1 + 625 \, U^2 / (L_{pp} \, \omega_e)^2} \qquad (136)$$

where L_{pp} is ship length between perpendiculars. The resulting roll damping coefficient including speed dependence is:

$$B_{44}^{hull-eddy} \quad = \quad \frac{B_{44}^{hull-eddy}(U)}{B_{44}^{hull-eddy}(0)} \; \frac{1}{4} \; \rho \; |\dot\eta_4| \; C_{eddy}^{hull} \int_{S_{hull}} n_4^2 \; \sqrt{y^2 \; + \; z^2} \; dS \quad (137)$$

For computations in the frequency domain, the equivalent linear damping coefficient based on energy dissipation is:

$$B_{44}^{hull-eddy} \quad = \quad \frac{B_{44}^{hull-eddy}(U)}{B_{44}^{hull-eddy}(0)} \; \frac{2}{3\pi} \; \rho \; \omega_e \; \hat\eta_4 \; C_{eddy}^{hull} \int_{S_{hull}} n_4^2 \; \sqrt{y^2 \; + \; z^2} \; dS \quad (138)$$

When computing ship motions in the time domain, the wave encounter frequency will often be varying with time. It is suggested that the ship roll natural frequency be used for the speed correction term in Equation (136) because roll damping is most important in the vicinity of roll resonance.

4.2   Drag Coefficient for Hull Eddy-Making Roll Damping

The method presented above requires selection of suitable value for the hull eddy damping coefficient C_{eddy}^{hull}. As noted above, the drag coefficient value of 1.17 for a flat plate is suggested as an initial estimate for the hull eddy damping coefficient. Experimental data can provide further insight into selection of suitable values for the coefficient C_{eddy}^{hull}.

4.3   Hull Skin Friction Roll Damping

Additional roll damping arises from flow tangential to the hull surface. The roll moment due to skin friction is given by:

$$F_4^{hull-skin} \quad = \quad \frac{1}{2} \; \rho \; |\dot\eta_4| \; \dot\eta_4 \; C_f^{hull} \int_{S_{hull}} (|y \; n_2| \; + |z \; n_3|)^2 \; \sqrt{y^2 \; + \; z^2} \; dS \quad (139)$$

The skin friction coefficient is calculated using the Schoenherr line for smooth turbulent flow:

$$C_f^{hull} \quad = \quad 0.0004 \; + \; \left[3.46 \log_{10} \left(\frac{U \; L_{pp}}{\nu} \right) \; - \; 5.6 \right]^{-2} \quad \text{for } U > 0 \quad (140)$$

For the case of zero forward speed, Schmitke [4] used an empirical equation from Kato [20] for the skin friction coefficient. To avoid discontinuities in skin friction coefficients at low speeds, a new approach is introduced here whereby a minimum

ship speed threshold is introduced for Equation (140). This approach is reasonable considering the slow variation of skin friction coefficient with ship speed. For a ship length of 100 m, a minimum ship speed of approximately 1 m/s is specified. Applying Froude scaling, the minimum input ship speed for Equation (140) is:

$$U_{min}(C_f^{hull}) \;=\; 0.03\sqrt{g\,L_{pp}} \tag{141}$$

The resulting roll damping coefficient arising from skin friction is:

$$B_{44}^{hull-skin} \;=\; \frac{1}{2}\,\rho\,|\dot{\eta}_4|\,C_f^{hull} \int_{S_{hull}} (|y\,n_2| + |z\,n_3|)^2 \sqrt{y^2 + z^2}\,dS \tag{142}$$

For computations in the frequency domain, the equivalent linear damping coefficient based on energy dissipation is:

$$B_{44}^{hull-skin} \;=\; \frac{4}{3\,\pi}\,\rho\,\omega_e\,\hat{\eta}_4\,C_f^{hull} \int_{S_{hull}} (y\,n_2 + z\,n_3)^2 \sqrt{y^2 + z^2}\,dS \tag{143}$$

5 Inclusion of Appendages in Hull Radiation and Diffraction Calculations

As stated in Section 3, ship appendages are normally assumed to have negligible influence on ship radiation and diffraction forces. This assumption greatly simplifies radiation and diffraction calculations, and is likely valid when appendages are deeply submerged and very small relative to the ship hull. In efforts to obtain improved ship motion predictions, a method has been developed to include appendages in hull radiation and diffraction calculations.

Computations for HMCS NIPIGON [6] showed that inclusion of appendages in hull radiation and diffraction calculations had negligible influence on predicted motions. However, appendage radiation and diffraction forces could be significant for ships with appendages that are larger or closer to the free surface.

5.1 Modelling of Appendages Using Dipole Panels

When computing hull radiation and diffraction forces in the frequency domain, the ShipMo3D library represents the wetted ship hull surface using a series of panels [1]. Flow boundary conditions on the hull are satisfied by solving for panel source strengths. Upon initial consideration, appendages could be included in the calculations by representing each appendage using source panels. Unfortunately, this approach is not practical due to the small thickness of the appendages relative to

practical panel sizes (see Sarpkaya and Isaacson [11]). Instead, the appendages can be assumed to be very thin, and represented using dipoles representing the flow across each panel. Sarpkaya and Isaacson [11], Chakrabarti [21], and Meyerhoff [22] provide useful references for computation of flows using dipole panels.

When including dipole appendages in radiation and diffraction computations, the approach for an unappended ship described in [1] must be modified. The velocity potential induced by a dipole panel is represented by:

$$\phi(\vec{x}) \quad = \quad \frac{1}{4\pi}\,\mu\,\int_{S_{dipole}} G^{dipole}(\vec{x}, \vec{x}_d, k_e)\,dS \qquad (144)$$

where $\vec{x}$ is the field point location, μ is the dipole strength, taken as being constant over the panel, S_{dipole} is the surface of the dipole, G^{dipole} is the frequency domain Green function for a dipole, $\vec{x}_d$ is the location on the dipole, and k_e is the wavenumber based on encounter frequency. The dipole strength μ is equal to the difference in source strength between the front and back of a dipole panel. The Green function for a dipole is related to the Green function for a source presented in Reference 1 as follows:

$$G^{dipole}(\vec{x}, \vec{x}_d, k_e) \quad = \quad \frac{\partial G(\vec{x}, \vec{x}_d, k_e)}{\partial n^{dipole}} \qquad (145)$$

where $G(\vec{x}, \vec{x}_d, k_e)$ is the Green function for a source and n^{dipole} is the normal vector from the dipole panel. The following equation is used for evaluating the normal derivative of the source Green function:

$$\frac{\partial G(\vec{x}, \vec{x}_d, k_e)}{\partial n^{dipole}} \quad = \quad \frac{\partial G(\vec{x}, \vec{x}_d, k_e)}{\partial n_x^{dipole}} + \frac{\partial G(\vec{x}, \vec{x}_d, k_e)}{\partial n_y^{dipole}} + \frac{\partial G(\vec{x}, \vec{x}_d, k_e)}{\partial n_z^{dipole}} \quad (146)$$

where n_x^{dipole}, n_y^{dipole}, and n_z^{dipole} are the directional components of the normal from the dipole panel. There are two possible choices for the normal directional from a dipole panel. The selected normal direction will determine the sign of the dipole strength μ computed for the panel.

As indicated by Meyeroff [22], the dipole strength μ must equal zero at the unbound edges of a thin appendage. This condition typically leads to high gradients in dipole strength near the edges; thus, it is often appropriate to have smaller panel sizes near the edges of an appendage.

As discussed by Sarpkaya and Isaacson [11], the only net pressure on a dipole panel arises from its own dipole strength. Other dipoles and sources induce equal pressures on both sides of the dipole, leading to a net pressure of zero across the dipole panel.

5.2 Derivatives of the Frequency Domain Green Function for a Source at Zero Forward Speed

As indicated above, the Green function for a dipole is based on the normal derivative of the Green function for a source. Note that derivatives are required for the Green function of a dipole; thus, second derivatives are required for the Green function of a source.

The ShipMo3D library uses the Telste and Noblesse [23] formulation of the Green function in the frequency domain at zero forward speed:

$$G(\vec{x}, \vec{x}_s, k_e) \;=\; \frac{1}{R} \;+\; \frac{1}{R_1} \;+\; \widetilde{G}_0(\vec{x}, \vec{x}_s, k_e) \tag{147}$$

where R is the distance from the field point $\vec{x}$ to the source at $\vec{x}_s$, R_1 is the distance from the field point $\vec{x}$ to the image of the source at $\vec{x}_s$, and $\widetilde{G}_0$ is the frequency dependent term of the Green function. Garrison [24] discusses the Green function at the zero and infinite frequency limits. The zero frequency (i.e., $k_e = 0$) limit is denoted $\overline{G}_0$ and given by:

$$\overline{G}_0(\vec{x}, \vec{x}_s, k_e) \;=\; \frac{1}{R} \;+\; \frac{1}{R_1} \text{ for } k_e = 0 \; (\omega_e = 0) \tag{148}$$

At infinite frequency (i.e., $k_e = \infty$), the Green function is denoted $\overline{G}_\infty$ and given by:

$$\overline{G}_\infty(\vec{x}, \vec{x}_s, k_e) \;=\; \frac{1}{R} \;-\; \frac{1}{R_1} \text{ for } k_e = \infty \; (\omega_e = \infty) \tag{149}$$

Accordingly, the frequency dependent portion $\widetilde{G}_0$ has the following limits:

$$\widetilde{G}_0(\vec{x}, \vec{x}_s, k_e) \;=\; 0 \text{ for } k_e = 0 \; (\omega_e = 0) \tag{150}$$

$$\widetilde{G}_0(\vec{x}, \vec{x}_s, k_e) \;=\; -\frac{2}{R_1} \text{ for } k_e = \infty \; (\omega_e = \infty) \tag{151}$$

Based on Telste and Noblesse, the frequency dependent term is expressed as follows:

$$\widetilde{G}_0(\vec{x}, \vec{x}_s, k_e) \;=\; 2 \, k_e \left[\widetilde{R_0}(h, v) - i \, \pi \, J_0(h) \, \exp(v) \right] \tag{152}$$

where $\widetilde{R_0}(h, v)$ is a function to be evaluated and $J_0(h)$ is the Bessel function of the first kind of order zero. The function arguments h and v are as follows:

$$R_{xy} \;=\; \sqrt{(x - x_s)^2 \;+\; (x - x_s)^2} \tag{153}$$

$$h \;=\; k_e \, R_{xy} \tag{154}$$

$$v \;=\; k_e \, (z \;+\; z_s) \tag{155}$$

Thus, R_{xy} is the horizontal distance from a field point to a source, h is the non-dimensional horizontal distance, and v is the non-dimensional elevation of the field point relative to the image of the source.

The derivatives of the Green function are required for computing flow velocities induced by a source. The zero frequency portion of the Green function has the following derivatives,

$$\frac{\partial \overline{G}_0}{\partial x} = \frac{-(x - x_s)}{R^3} - \frac{(x - x_s)}{R_1^3} \tag{156}$$

$$\frac{\partial \overline{G}_0}{\partial y} = \frac{-(y - y_s)}{R^3} - \frac{(y - y_s)}{R_1^3} \tag{157}$$

$$\frac{\partial \overline{G}_0}{\partial z} = \frac{-(z - z_s)}{R^3} - \frac{(z + z_s)}{R_1^3} \tag{158}$$

Teltse and Noblesse give the following equations for the derivatives of the frequency dependent portion of the Green function

$$\frac{\partial \widetilde{G}_0}{\partial R_{xy}} = -2k_e^2 \left[\widetilde{R}_1(h, v) - i\pi J_1(h) \exp(v) \right] \tag{159}$$

$$\frac{\partial \widetilde{G}_0}{\partial x} = \frac{\partial R_{xy}}{\partial x} \frac{\partial \widetilde{G}}{\partial R_{xy}} \tag{160}$$

$$\frac{\partial \widetilde{G}_0}{\partial y} = \frac{\partial R_{xy}}{\partial y} \frac{\partial \widetilde{G}}{\partial R_{xy}} \tag{161}$$

$$\frac{\partial \widetilde{G}_0}{\partial z} = 2k_e^2 \left[\frac{1}{k_e R_1} + \widetilde{R}_0(h, v) - i\pi J_0(h) \exp(v) \right] \tag{162}$$

where $\widetilde{R}_1(h, v)$ is a function to be evaluated, and $J_1(h)$ is the Bessel function of the first kind of order one. The derivatives of R_{xy} with respect to x and y are:

$$\frac{\partial R_{xy}}{\partial x} = \frac{(x - x_s)}{R_{xy}} \tag{163}$$

$$\frac{\partial R_{xy}}{\partial y} = \frac{(y - y_s)}{R_{xy}} \tag{164}$$

When evaluating the flow velocities induced by a dipole, the second derivatives of the Green function are required. Relevant terms are:

$$\frac{\partial^2 \widetilde{G}_0}{\partial R_{xy}^2} = -2k^3 \left[\frac{\partial \widetilde{R}_1(h, v)}{\partial h} - i\pi \frac{\partial J_1(h)}{\partial h} \exp(v) \right] \tag{165}$$

$$\frac{\partial^2 \widetilde{G}_0}{\partial x^2} \;=\; \frac{\partial^2 R_{xy}}{\partial x^2}\,\frac{\partial \widetilde{G}}{\partial R_{xy}} \;+\; \left(\frac{\partial R_{xy}}{\partial x}\right)^2 \frac{\partial^2 \widetilde{G}}{\partial R_{xy}^2} \tag{166}$$

$$\frac{\partial^2 \widetilde{G}_0}{\partial x \partial y} \;=\; \frac{\partial^2 R_{xy}}{\partial x \partial y}\,\frac{\partial \widetilde{G}}{\partial R_{xy}} \;+\; \frac{\partial R_{xy}}{\partial x}\,\frac{\partial R_{xy}}{\partial y}\,\frac{\partial^2 \widetilde{G}}{\partial R_{xy}^2} \tag{167}$$

$$\frac{\partial^2 \widetilde{G}_0}{\partial y^2} \;=\; \frac{\partial^2 R_{xy}}{\partial y^2}\,\frac{\partial \widetilde{G}}{\partial R_{xy}} \;+\; \left(\frac{\partial R_{xy}}{\partial y}\right)^2 \frac{\partial^2 \widetilde{G}}{\partial R_{xy}^2} \tag{168}$$

$$\frac{\partial^2 \widetilde{G}_0}{\partial R_{xy} \partial z} \;=\; 2k^3 \left[\frac{1}{k_e}\frac{\partial}{\partial R_{xy}}\frac{1}{R_1} \;-\; k_e\,\widetilde{R}_1(h,v) \;+\; i\,\pi\,k_e\,J_1(h)\,\exp v \right] \tag{169}$$

$$\frac{\partial^2 \widetilde{G}_0}{\partial x \partial z} \;=\; \frac{\partial R_{xy}}{\partial x}\,\frac{\partial^2 \widetilde{G}_0}{\partial R_{xy} \partial z} \tag{170}$$

$$\frac{\partial^2 \widetilde{G}_0}{\partial y \partial z} \;=\; \frac{\partial R_{xy}}{\partial y}\,\frac{\partial^2 \widetilde{G}_0}{\partial R_{xy} \partial z} \tag{171}$$

$$\frac{\partial^2 \widetilde{G}_0}{\partial z^2} \;=\; 2k_e^2 \left[\frac{1}{k_e}\frac{\partial}{\partial z}\frac{1}{R_1} \;+\; k_e\frac{\partial \widetilde{R}_0(h,v)}{\partial v} \;-\; i\,\pi\,J_0(h)\,k_e\,\exp(v) \right] \tag{172}$$

The second derivatives of R_{xy} are:

$$\frac{\partial R_{xy}^2}{\partial x^2} \;=\; \frac{1}{R_{xy}} \;-\; \frac{(x-x_s)^2}{R_{xy}^2} \tag{173}$$

$$\frac{\partial R_{xy}^2}{\partial x\,\partial y} \;=\; -\,\frac{(x-x_s)\,(y-y_s)}{R_{xy}^3} \tag{174}$$

$$\frac{\partial R_{xy}^2}{\partial y^2} \;=\; \frac{1}{R_{xy}} \;-\; \frac{(y-y_s)^2}{R_{xy}^2} \tag{175}$$

The above equations utilize the following relation given by Telste and Noblesse:

$$\frac{\partial \widetilde{R}_0(h,v)}{\partial h} \;=\; -\,\widetilde{R}_1(h,v) \tag{176}$$

The derivatives $\partial \widetilde{R}_0(h,v)/\partial v$ and $\partial \widetilde{R}_1(h,v)/\partial h$ are evaluated using finite difference methods, which allow utilization of the fast algorithms of Telste and Noblesse. The Bessel function derivative $\partial J_1(h)/\partial h$ is given by:

$$\frac{\partial J_1(h)}{\partial h} \;=\; J_0(h) \;-\; \frac{J_1(h)}{h} \ \text{for } h > 0 \tag{177}$$

$$=\; 0.5 \ \text{for } h = 0 \tag{178}$$

5.3 Algebraic Solution of Hull Source and Appendage Dipole Strengths

The solution of hull source and appendage dipole strengths is very similar to the approach used for a hull alone represented by source panels in Reference 1. Lateral symmetry is utilized to reduce the required computational time. Special care must be taken if a ship includes vertical appendages on the centreline, such as a skeg or single rudder. For longitudinal modes, the dipole strengths on centreline appendages are zero; thus, centreline dipole strength terms should be excluded when solving for longitudinal modes.

5.4 Verification of Radiation Computations for Appended Hull

To verify radiation computations for a hull with appendages, sway added mass has been evaluated for a thin box with length of 20 m, depth of 10 m, and width of 0.4 m. A first set of computations models the box as a hull with no appendages. A second set of computations models the upper half as a box and the lower half as a thin plate. Figure 11 shows the two different configurations, denoted as "Box" and "Box-plate". For both configurations, there are 20 panels along the length of the body and 20 panels along the total depth of the body.

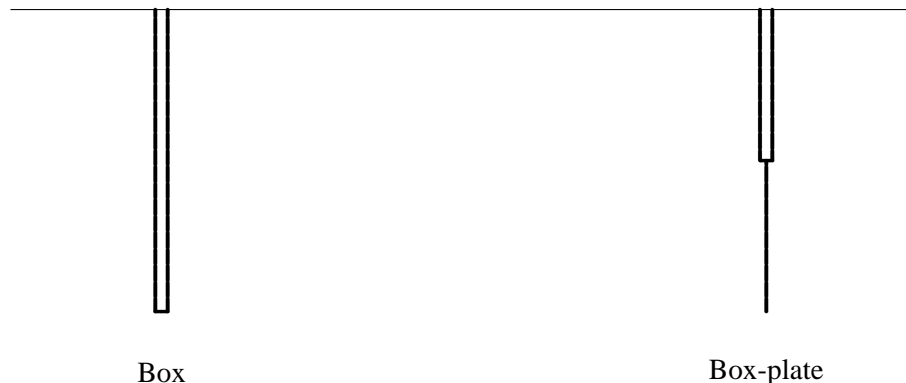Box   Box-plate

Figure 11: Cross-Sections of Thin Box for Verification of Radiation Computations with Appended Hull

The computed added mass and damping coefficients in Figures 12 and 13 show reasonable agreement considering that the modelled geometries are somewhat dif-

ferent. This agreement suggests that the radiation computations using dipole appendage panels have been implemented correctly.

6 Control of Rudder Deflections with a Simple Autopilot

The lateral motions of a ship in waves will be influenced by rudder deflections, which are often driven by an autopilot. This section presents a relatively simple autopilot, and provides a starting point for simulation of rudder motions. Future studies will investigate more complex helm control systems.

In response to ship motions, a rudder will deflect according to prescribed motion gains and the response characteristics of the rudder system. Equations of rudder motions are presented in various references, including References 10 and 12. The commanded rudder deflection angle determined by the ship motions and autopilot gains is as follows:

$$\delta_C^{rudder} \;=\; \sum_{j=1}^{j} \left(k_{\delta j}^a \; \ddot{\eta}_j \;+\; k_{\delta j}^v \; \dot{\eta}_j \;+\; k_{\delta j}^d \; \eta_j \right) \tag{179}$$

where $k_{\delta j}^a$ is the acceleration gain for motion mode j, $k_{\delta j}^v$ is the velocity gain, and $k_{\delta j}^d$ is the displacement gain. The rudder response characteristics are modelled as follows:

$$\ddot{\delta}^{rudder} \;+\; 2\,\zeta_\delta\,\omega_\delta^{rudder}\,\dot{\delta}^{rudder} \;+\; \omega_\delta^2\,\delta^{rudder} \;=\; \omega_\delta^2\,\delta_C^{rudder} \tag{180}$$

where ζ_δ is nondimensional damping response constant, and $\omega_{\delta j}$ is the rudder frequency response constant. The rudder motions in the time domain can be easily evaluated as follows:

$$\ddot{\delta}^{rudder} \;=\; \omega_\delta^2 \left(\delta_C^{rudder} \;-\; \delta^{rudder} \right) - \; 2\,\zeta_\delta\,\omega_\delta\,\dot{\delta}^{rudder} \tag{181}$$

Motions in the frequency domain are evaluated using the following coupled equation of ship and rudder motions:

$$\left[\begin{array}{c|c} M_{\eta\eta}^e & 0 \\ \hline M_{\delta\eta}^e & M_{\delta\delta}^e \end{array} \right] \left\{ \begin{array}{c} \ddot{\eta} \\ \ddot{\delta}^{rudder} \end{array} \right\} \;+\; \left[\begin{array}{c|c} B_{\eta\eta} & 0 \\ \hline B_{\delta\eta} & B_{\delta\delta} \end{array} \right] \left\{ \begin{array}{c} \dot{\eta} \\ \dot{\delta}^{rudder} \end{array} \right\} \tag{182}$$

$$+\; \left[\begin{array}{c|c} C_{\eta\eta} & C_{\eta\delta} \\ \hline C_{\delta\eta} & C_{\delta\delta} \end{array} \right] \left\{ \begin{array}{c} \eta \\ \delta^{rudder} \end{array} \right\} = \left\{ \begin{array}{c} F_\eta \\ 0 \end{array} \right\}$$

The matrices and vectors in the above equation are partitioned into ship motion and rudder deflection portions, and the effective mass matrix $[M^e]$ includes contributions from both ship mass and added mass. Terms for the influence of rudder
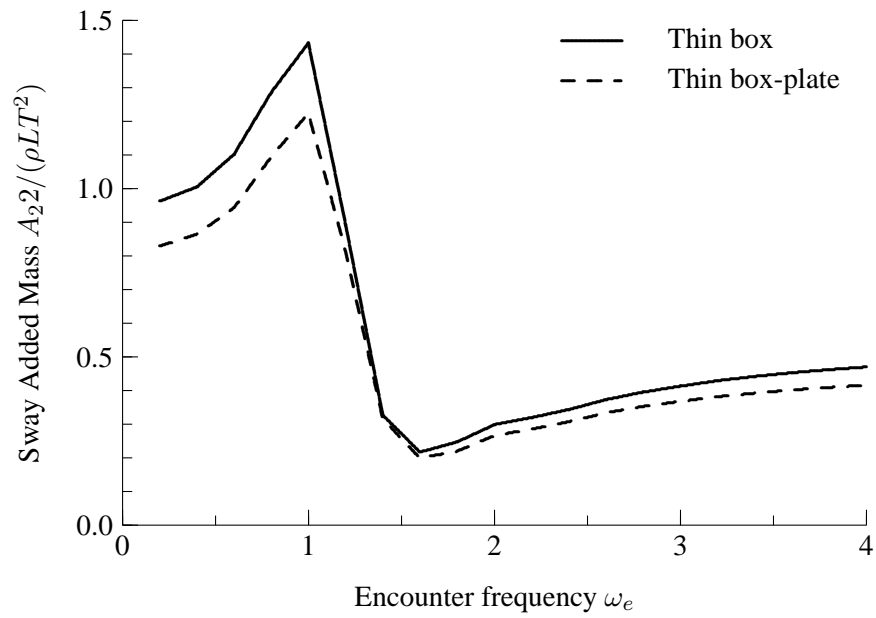
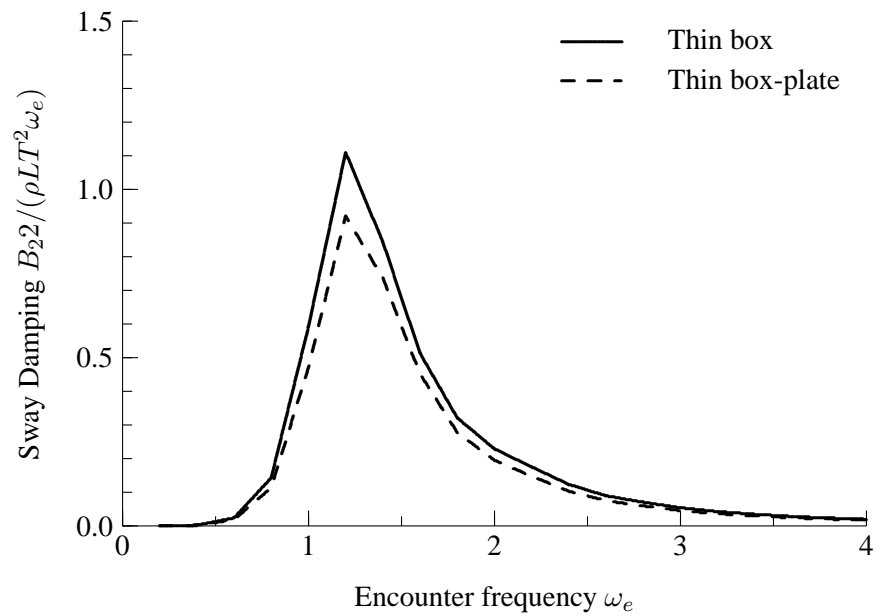***Figure 12:*** *Sway Added Mass for Thin Box and Thin Box with Appended Plate*

Figure 13: *Sway Damping for Thin Box and Thin Box with Appended Plate*

deflections on ship motions were previously given in Section 3. Other terms are as follows:

$$M_{\delta j}^e = -\omega_\delta^2 \, k_{\delta j}^a \tag{183}$$

$$M_{\delta\delta}^e = 1 \tag{184}$$

$$B_{\delta j} = -\omega_\delta^2 \, k_{\delta j}^v \tag{185}$$

$$B_{\delta\delta} = 2 \, \zeta_\delta \, \omega_\delta \tag{186}$$

$$C_{\delta j} = -\omega_\delta^2 \, k_{\delta j}^d \tag{187}$$

$$C_{\delta\delta} = \omega_\delta^2 \tag{188}$$

The simulation of a rudder control system including autopilot requires selection of suitable input values. For a US Coast Guard cutter representative of modern frigate design, Smith [25] indicates a maximum rudder deflection of 35 degrees and maximum rudder rate of 3 degrees per second. For modelling of a conventional downward rudder using ShipMo3D, yaw gain and yaw velocity gain will typically have values greater than zero. Values reported by Smith indicate that yaw autopilot gains fitted to observed human pilot behaviour will have a wide range of variation.

7 Numerical Implementation

As with other components of the ShipMo3D library, the present work has been implemented using the Python programming language [26, 27]. Python is a high level, object-oriented language that has a significant user base among the scientific community. The ShipMo3D library uses the Numeric Python library [28] which provides fast computational speed for numerical operations. The scientific Python module SciPy (www.scipy.org) provides additional routines such as fast solution of systems of linear equations.

7.1 Convergence to Correct Roll Amplitude for Frequency Domain Computations

When evaluating roll motions in the frequency domain, an iterative procedure must be used to determine the correct roll amplitude for roll damping computations. Convergence is obtained when the following is satisfied:

$$\left| \hat{\eta}_4(\hat{\eta}_4^{damping}) \, - \, \hat{\eta}_4^{damping} \right| \; \leq \; \epsilon^{tol}(\hat{\eta}_4) \tag{189}$$

where $\hat{\eta}_4(\hat{\eta}_4^{damping})$ is the computed roll amplitude based on roll damping for roll amplitude $\hat{\eta}_4^{damping}$, and $\epsilon^{tol}(\hat{\eta}_4)$ is the tolerance on roll damping amplitude. To

ensure repeatability of calculations, a small tolerance should be used for roll amplitude, and a value of 0.0001 degrees has been selected.

As an illustrative example, Figure 14 shows the variation of computed roll amplitude with roll amplitude used for determining nonlinear roll damping. The present case has significant roll resonance, causing predicted roll amplitude to be very dependent on the roll amplitude used for computing damping. Figure 14 also shows the line $\hat{\eta}_4(\hat{\eta}_4^{damping}) = \hat{\eta}_4^{damping}$. The correct solution is at the intersection of the two lines.
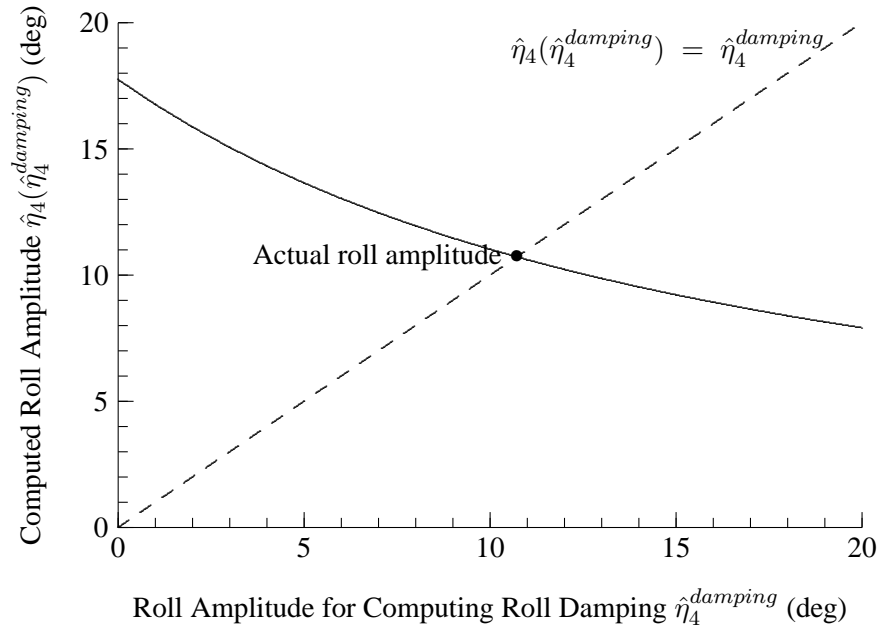

Figure 14: *Computed Roll Amplitude Versus Roll Amplitude for Computing Damping, Frigate in Regular Waves*

Iterative procedures for roll amplitude often employ the simple method of using the computed roll amplitude from the previous iteration for computing roll damping. This approach neglects the variation of $\hat{\eta}_4(\hat{\eta}_4^{damping})$ with $\hat{\eta}_4$ when determining the next value for $\hat{\eta}_4^{damping}$. Much faster convergence can be achieved by considering the variation of $\hat{\eta}_4(\hat{\eta}_4^{damping})$ with $\hat{\eta}_4^{damping}$, applying the following increment to $\hat{\eta}_4^{damping}$ in a given iteration:

$$\Delta\hat{\eta}_4^{damping} = \frac{\hat{\eta}_4(\hat{\eta}_4^{damping}) - \hat{\eta}_4^{damping}}{1 - \partial\hat{\eta}_4(\hat{\eta}_4^{damping})/\partial\hat{\eta}_4^{damping}} \tag{190}$$

The term $\partial\hat{\eta}_4(\hat{\eta}_4^{damping})/\partial\hat{\eta}_4^{damping}$ is evaluated using a secant method based on linear interpolation of computed values of $\hat{\eta}_4(\hat{\eta}_4^{damping})$ from previous iterations. If

no values are available from previous iterations, then $\partial \hat{\eta}_4(\hat{\eta}_4^{damping})/\partial \hat{\eta}_4^{damping}$ is assumed to be zero.

Faster convergence is achieved if the first iteration is based on a reasonable initial guess of roll amplitude. In long waves, the ship roll amplitude is given by:

$$\hat{\eta}_4 \;\; = \;\; k_I \, a \, |\sin \beta| \tag{191}$$

where k_I is the wavenumber of incident waves. In short waves, the roll amplitude goes to zero. The following equation has been developed based on computed roll motions for the initial guess of roll amplitude:

$$\hat{\eta}_4 \;\; \approx \;\; k_I \, a \, |\sin \beta| \, \exp\left(-0.08 \, L_{pp} \, k_I\right) \tag{192}$$

The above procedure has been found to be very stable and efficient, with convergence usually achieved within 8 iterations. For frequency domain computations for random seas, the roll amplitude for roll damping computations is taken as 1.25 times the RMS roll.

8 Validation of Roll Damping and Motion Predictions with the Haslar Steered Warship Model

Experiments for the steered warship model of Lloyd and Crossland [29] have been selected for validating roll damping and motion predictions from the ShipMo3D library. These experiments were conducted in the Manoeuvring Tank at Admiralty Research Establishment Haslar (now part of the privatized QinetiQ). Lloyd and Crossland's experiments were selected for the present validation because they include comprehensive measurements of both ship motions and rudder motions, which were driven by an autopilot with documented properties. The results reported here include conditions that were not documented in Reference 29, for which the data were provided directly to DRDC Atlantic.

Table 2 gives the particulars for the steered warship model, and Figure 15 shows the body plan. Tables 3 to 6 give dimensions for the bilge keels, propeller shaft brackets, stabilizer fins, and rudders. Some of the longitudinal locations of appendages in Tables 3 to 6 have corrections from those originally presented in Reference 29. The steered warship model included an autopilot with control parameters as given in Table 7.

Table 2: *Main Particulars for Haslar Steered Warship Model*

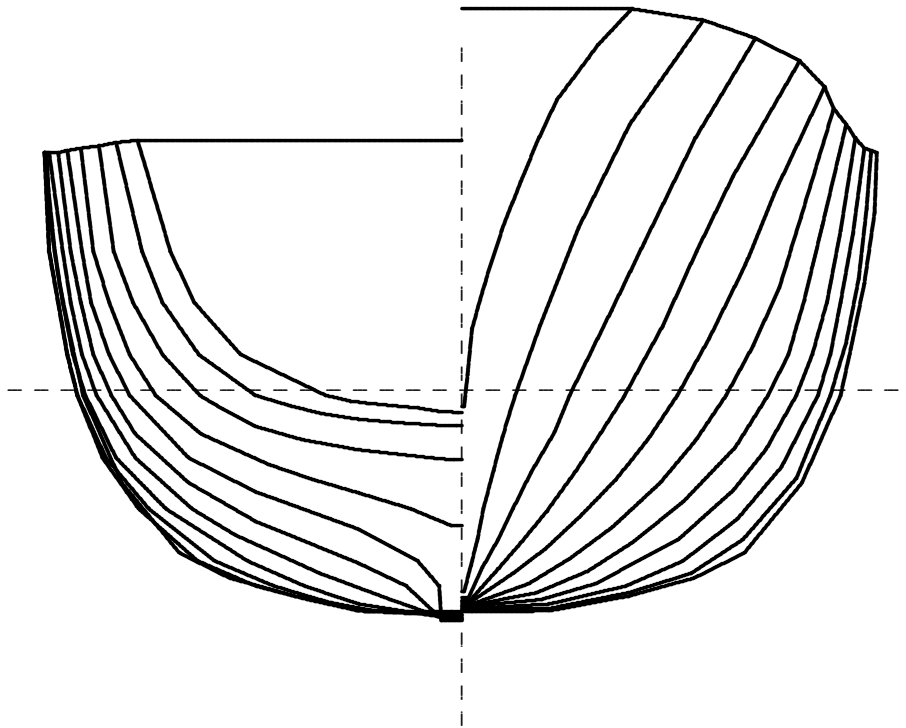|	
Length, L_{pp}	5580 mm
Beam, B	671 mm
Midships draft, T_{mid}	196 mm
Trim by stern, t_s	0 mm
Displacement, $\triangle$	345 kg
Vertical centre of gravity, $\overline{KG}$	276 mm
Metacentric height, $\overline{GM}_{fluid}$	76 mm
Roll radius of gyration, r_{xx}	257 mm
Pitch radius of gyration, r_{yy}	1293 mm
Yaw radius of gyration, r_{zz}	1265 mm

Figure 15: *Body Plan for Haslar Steered Warship Model*

Table 3: *Bilge Keel Dimensions for Haslar Steered Warship Model*

Station (20 at AP)	6.79	7	8	9	9.69
Span (mm)	68	68	68	68	68
Root lateral offset (mm)	239	239	243	248	248
Root above baseline (mm)	107	107	82	64	64
Dihedral angle (deg, port side)	-45	-45	-45	-45	-45

Table 4: *Propeller Shaft Bracket Dimensions for Haslar Steered Warship Model*

	Aft inner bracket	Aft outer bracket	Fore inner bracket	Fore outer bracket
Station (20 at AP)	18.40	18.40	17.97	17.97
Span (mm)	165	127	81	68
Root chord (mm)	30	30	12	12
Tip chord (mm)	30	30	12	12
Root lateral offset (mm)	21	132	72	157
Root above baseline (mm)	148	163	103	125
Dihedral angle (deg, port side)	-47.5	-99.5	-42	-90

Table 5: *Stabilizer Fin Dimensions for Haslar Steered Warship Model*

Station (20 at AP)	10.38
Span (mm)	83
Root chord (mm)	174
Tip chord (mm)	92
Root lateral offset (mm)	273
Root above baseline (mm)	75
Dihedral angle (deg, port side)	-46

Table 6: *Rudder Dimensions for Haslar Steered Warship Model*

Station (20 at AP)	19.46
Span (mm)	153
Root chord (mm)	124
Tip chord (mm)	88
Root lateral offset (mm)	79
Root above baseline (mm)	178
Dihedral angle (deg, port side)	-83

Table 7: *Rudder Control Properties for Haslar Steered Warship Model*

Maximum deflection angle δ_{max}^{rudder}	35 deg
Maximum deflection rate $\dot{\delta}_{max}^{rudder}$	35 deg/s
Deflection natural frequency ω_δ	25.8 rad/s
Deflection damping ratio ζ_δ	0.85
Yaw displacement gain $k_{\delta 6}^d$	3.8
Yaw velocity gain $k_{\delta 6}^v$	1.7 s
Yaw acceleration gain $k_{\delta 6}^a$	0.0 s^2

For experimental sway motions, Reference 29 describes a procedure for conversion from body axes to earth fixed axes. The present report uses experimental sway motions without this correction because it is doubtful that the correction is applicable for sway motions measured using an accelerometer, as was done during the model tests.

8.1   Roll Damping in Calm Water

The Halsar steered warship experiments included roll decay tests in calm water. ShipMo3D predictions of the experimental conditions have been made using the following methods for bilge keel drag coefficients:

- Ikeda's method (Equation (125)),

- the simplified Kato method based on roll amplitude (Equation (129)).

Figures 16 to 23 indicate that roll damping tends to be underpredicted when using Ikeda's method, and overpredicted when using the simplified Kato method. The presented roll damping values are normalized by the critical roll damping value B_{44}^{cr}. When considering which of the two methods is more accurate for predicting bilge keel drag coefficients, it should be noted that there is greater uncertainty with predicted roll forces as ship speed increases, in part due to violation of the assumption of low speed when computing hull radiation forces. Consequently, roll damping decay tests at lower speeds are likely more appropriate for determining which method provides more accurate predictions of bilge keel drag coefficients. Figures 16 to 20, which include Froude numbers up to 0.18, suggest that Ikeda's method is more accurate than the simplified Kato method for predicting bilge keel drag coefficients.
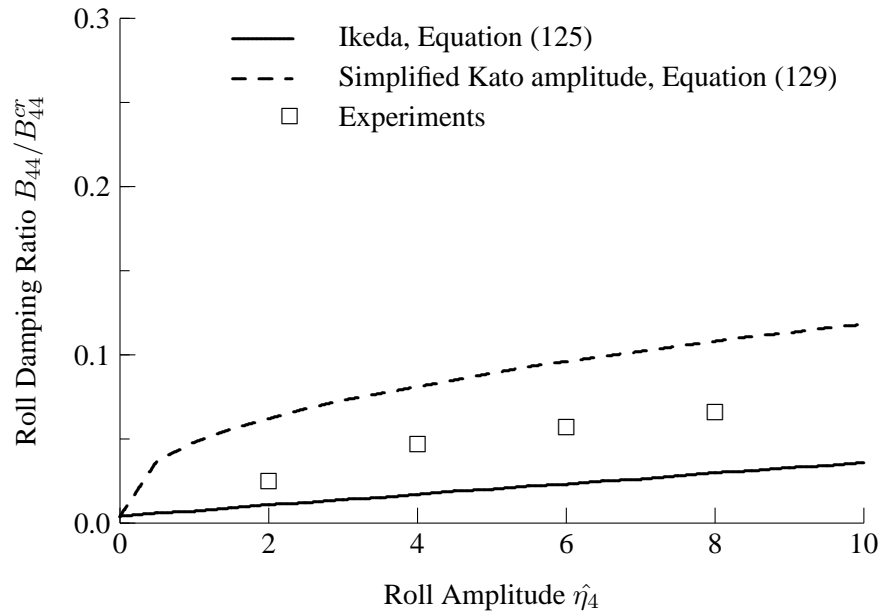
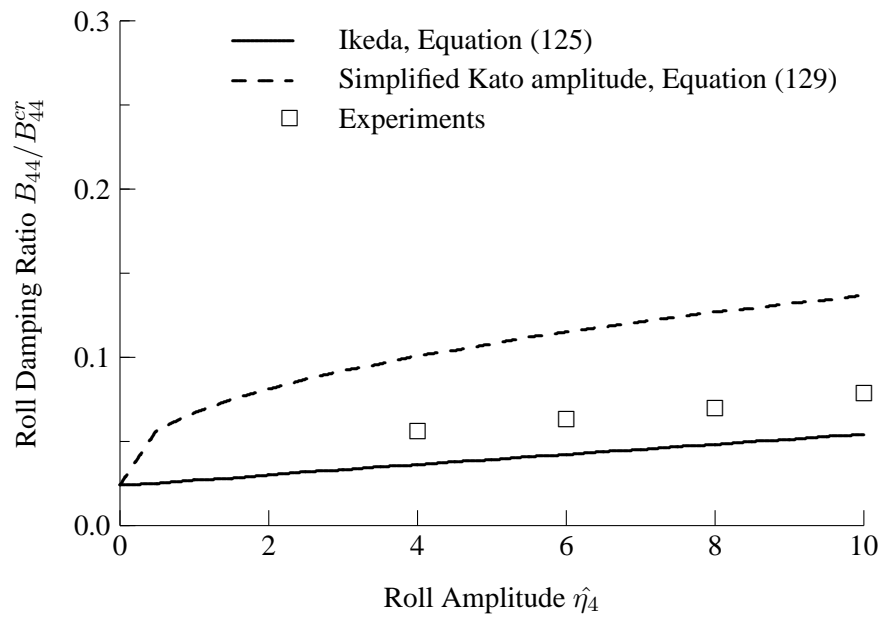**Figure 16:** *Roll Damping Steered Warship, Froude Number = 0.00*

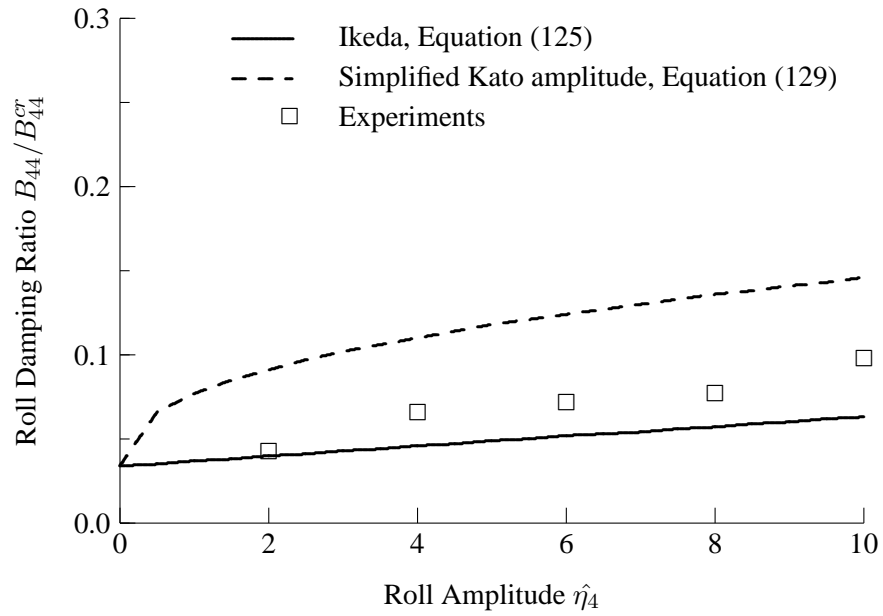**Figure 17:** *Roll Damping Steered Warship, Froude Number = 0.06*

Figure 18: *Roll Damping Steered Warship, Froude Number = 0.09*
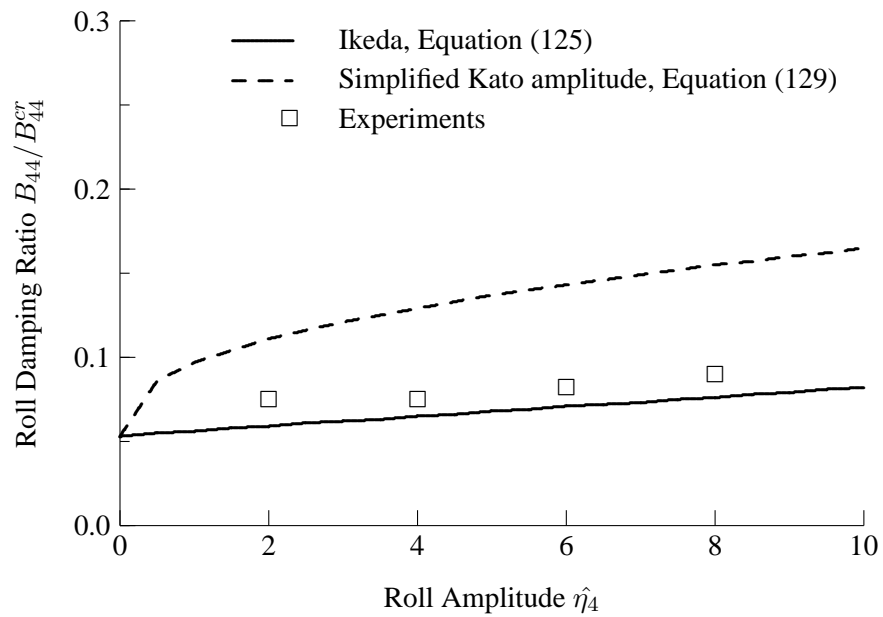

Figure 19: *Roll Damping Steered Warship, Froude Number = 0.15*
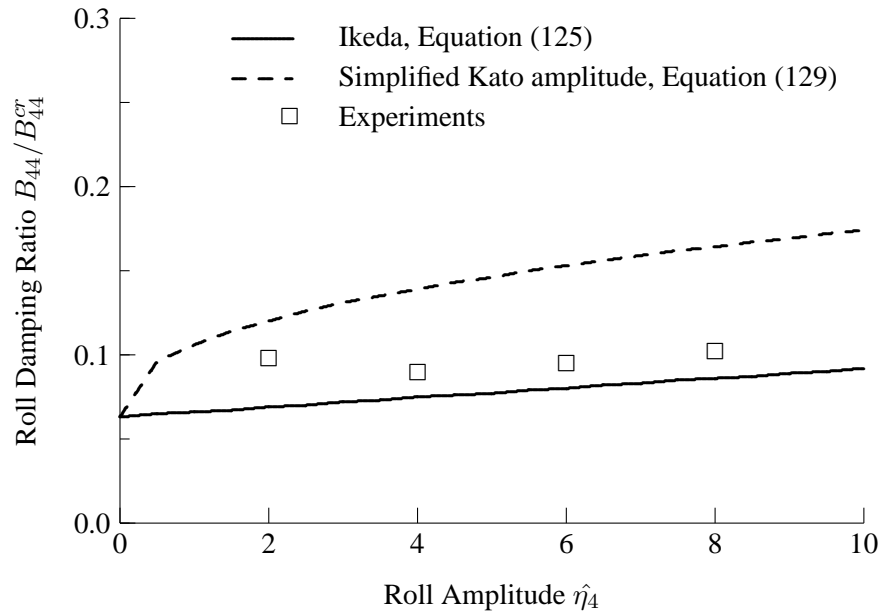
Figure 20: *Roll Damping Steered Warship, Froude Number = 0.18*
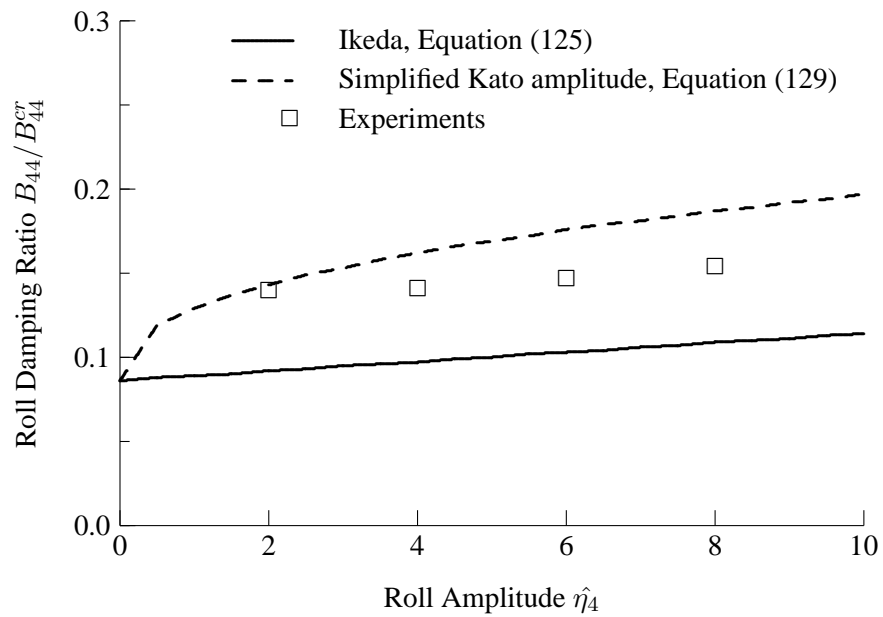

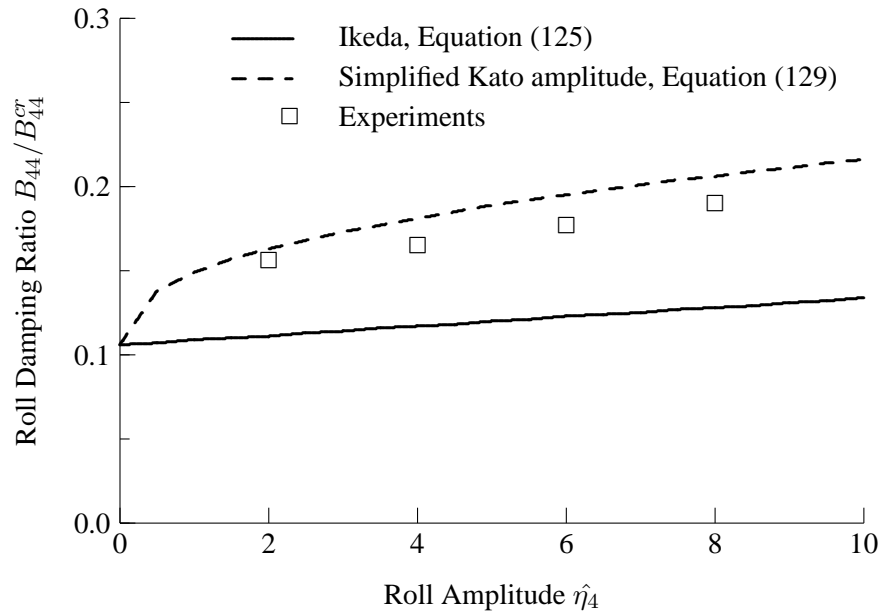**Figure 21:** *Roll Damping Steered Warship, Froude Number = 0.25*

Figure 22: *Roll Damping Steered Warship, Froude Number = 0.31*
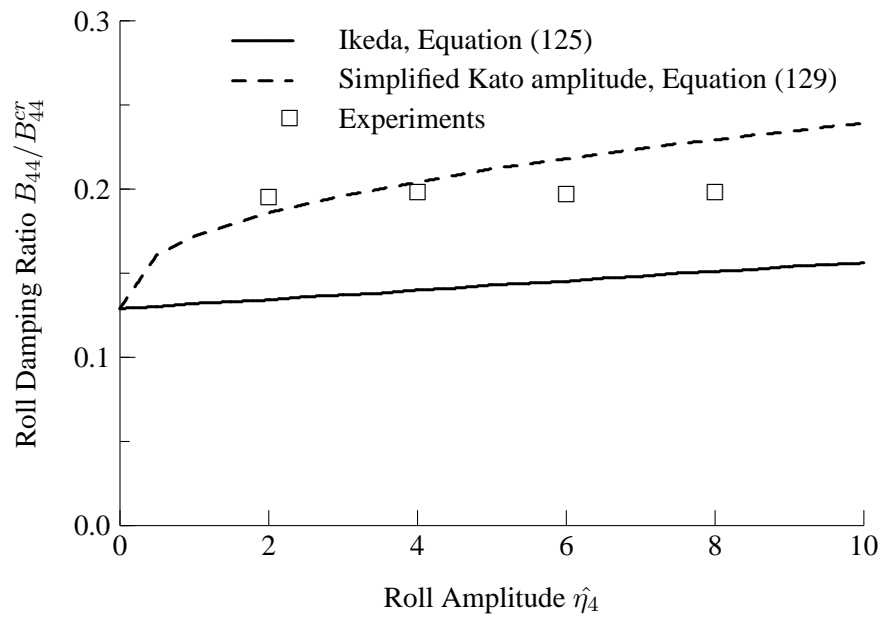

Figure 23: *Roll Damping Steered Warship, Froude Number = 0.38*

8.2 Roll Motions in Beam Seas Using Different Methods for Bilge Keel Drag Coefficients

Roll motions have been computed in beam seas using the following 3 methods for predicting bilge keel drag coefficients:

- Ikeda's method, Equation (125),

- the simplified Kato method based on roll velocity, Equation (127).

- the simplified Kato method based on roll amplitude, Equation (129).

A primary motivation for the comparison was to determine if bilge keel drag coefficients depend on roll amplitude as suggested by Ikeda et al. [19], or on roll velocity as suggested by Kato [14]. Figures 24, 25 and 26 show roll motions in beam waves for Froude numbers of 0.18, 0.28, and 0.36. Figure 24 indicates that Ikeda's method provides the best roll motion predictions, while the two approaches based on Kato lead to underprediction of roll motions. The interpretation of results at higher speeds is more difficult, in part due to the greater difficulty in predicting hull radiation and diffraction forces as ship speed increases.
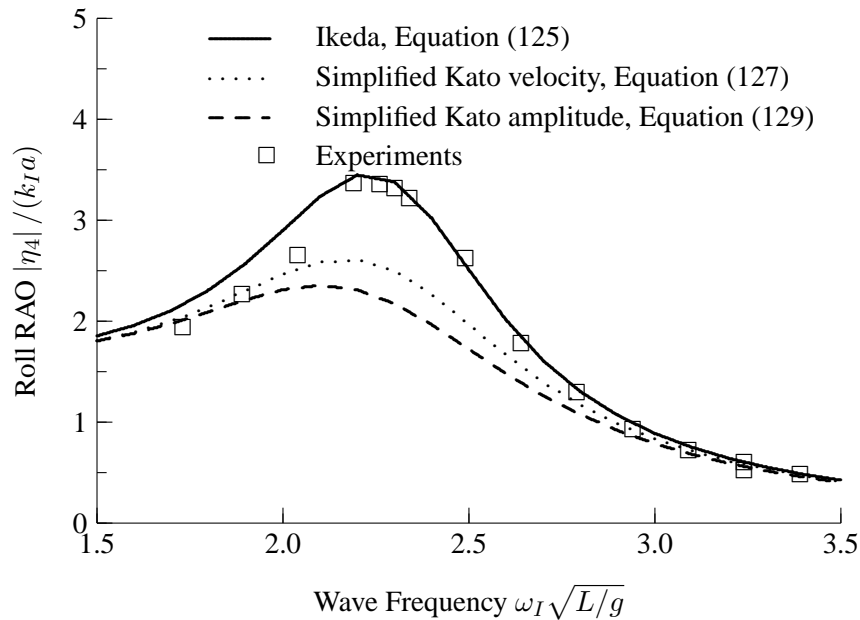

Figure 24: *Roll RAOs for Steered Warship with Different Bilge Keel Drag Coefficients, Beam Seas, Froude Number 0.18*
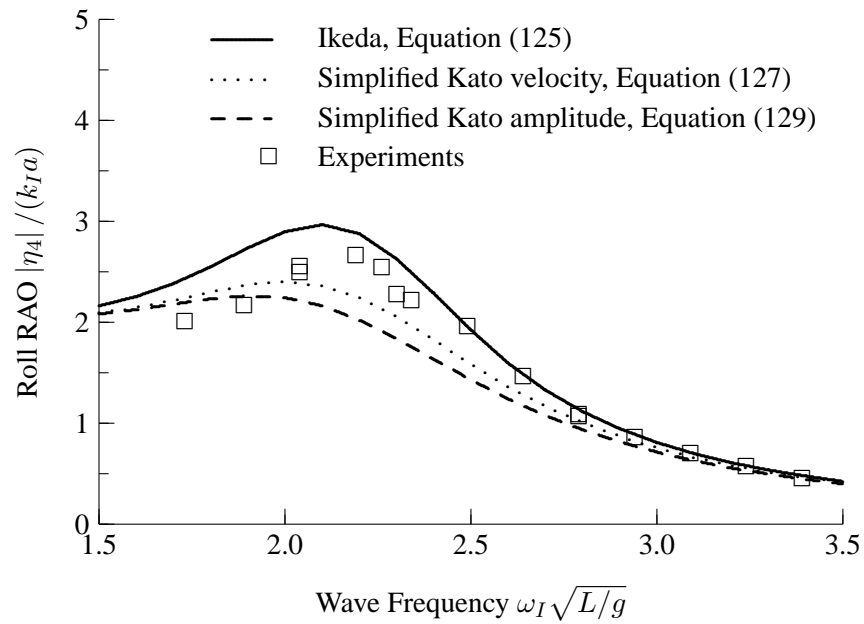
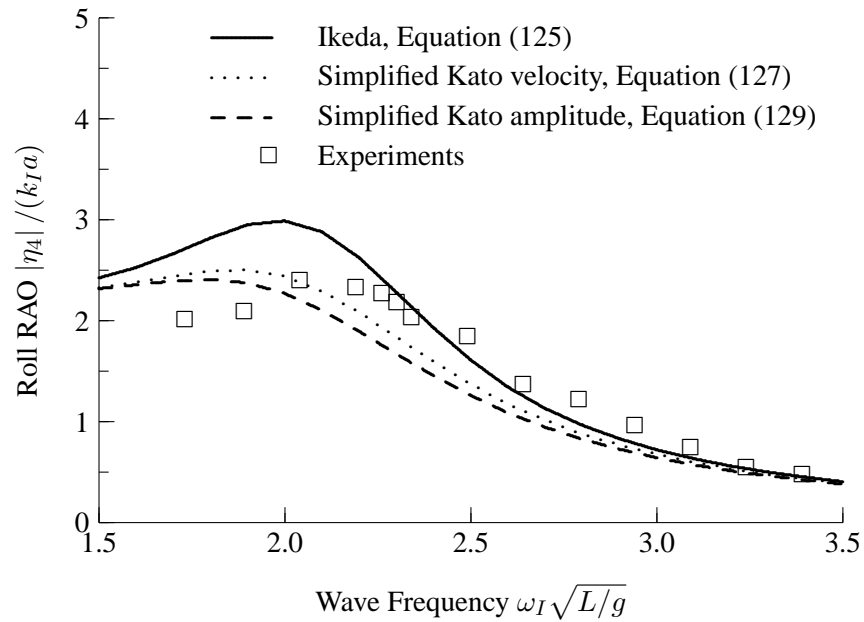**Figure 25:** *Roll RAOs for Steered Warship with Different Bilge Keel Drag Coefficients, Beam Seas, Froude Number 0.28*

Figure 26: *Roll RAOs for Steered Warship with Different Bilge Keel Drag Coefficients, Beam Seas, Froude Number 0.36*

8.3 Motion Predictions in All Experimental Conditions

Figures 27 to 43 show comparisons of predictions and experiments for all available experimental conditions. The numerical predictions include ShipMo3D time domain, ShipMo3D frequency domain, and the strip theory frequency domain program SHIPMO7 [8]. The ShipMo3D predictions use Ikeda's method for bilge keel drag coefficients. SHIPMO7 uses Kato's method for predicting bilge keel drag coefficients.

The numerical predictions from both the ShipMo3D library and from SHIPMO7 give generally good agreement with the experiments. The excellent agreement between frequency domain and time domain results from ShipMo3D indicate consistency between the frequency domain and time domain simulations. The similarity of predictions from ShipMo3D and SHIPMO7 is likely due to slenderness of the hull geometry. As expected, the numerical predictions are better for heave and pitch than for sway, roll, and yaw.

Agreement between predictions and experiments generally decreases as ship speed increases, likely due to the assumption of low forward ship speed in the radiation and diffraction computations. The absence of hull lift forces in the present ShipMo3D predictions will also affect accuracy at higher ship speeds. The correspondence of trends for yaw and rudder predictions suggests that the rudder response to yaw motions is being correctly modelled.

Figure 27: *RAOs for Steered Warship, Stern Quartering Seas at 0 degrees, Froude Number 0.28*

Figure 28: *RAOs for Steered Warship, Stern Quartering Seas at 0 degrees, Froude Number 0.37*

Figure 29: *RAOs for Steered Warship, Stern Quartering Seas at 30 degrees, Froude Number 0.18*

Figure 30: *RAOs for Steered Warship, Stern Quartering Seas at 30 degrees, Froude Number 0.27*
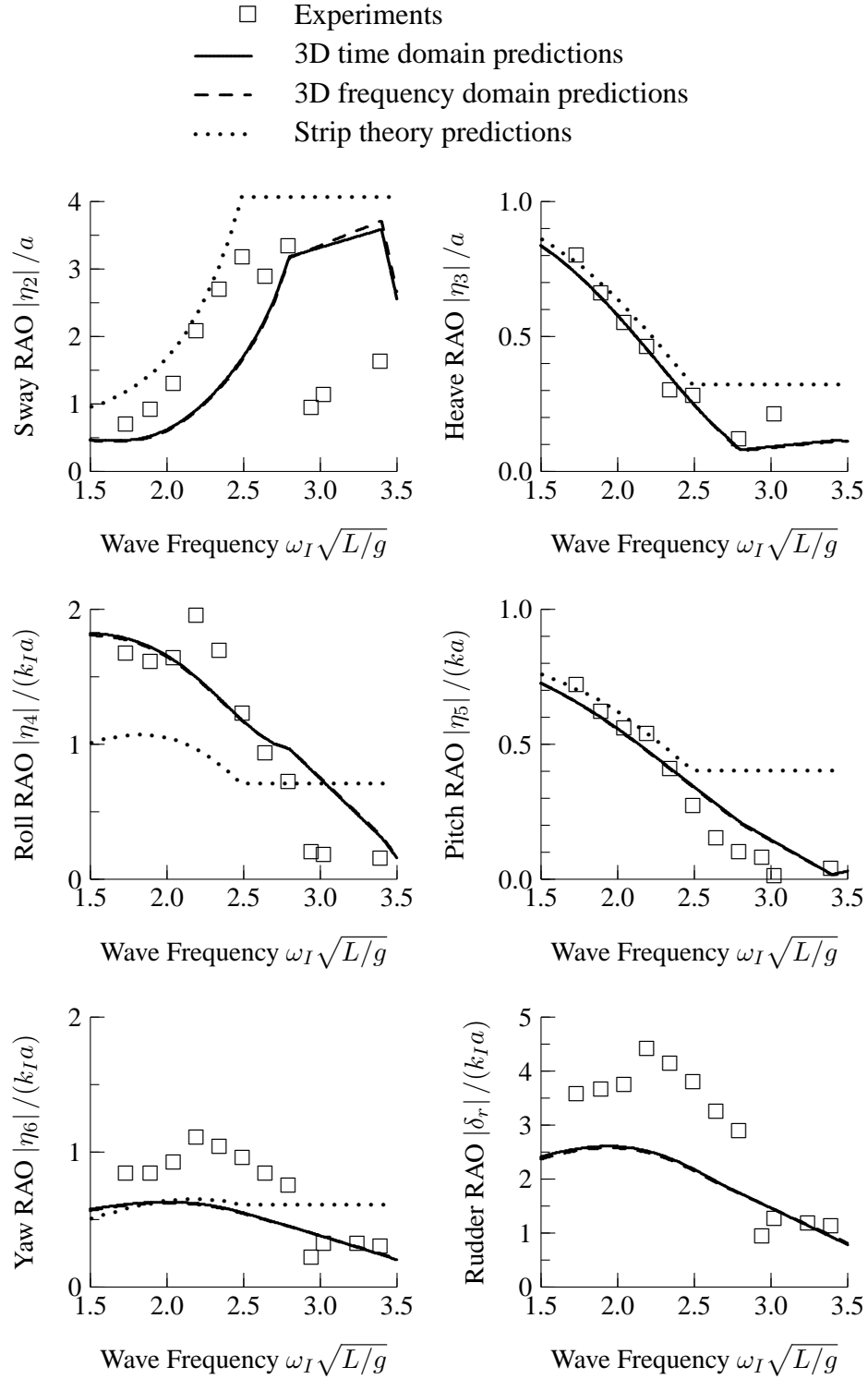
Figure 31: *RAOs for Steered Warship, Stern Quartering Seas at 30 degrees, Froude Number 0.37*
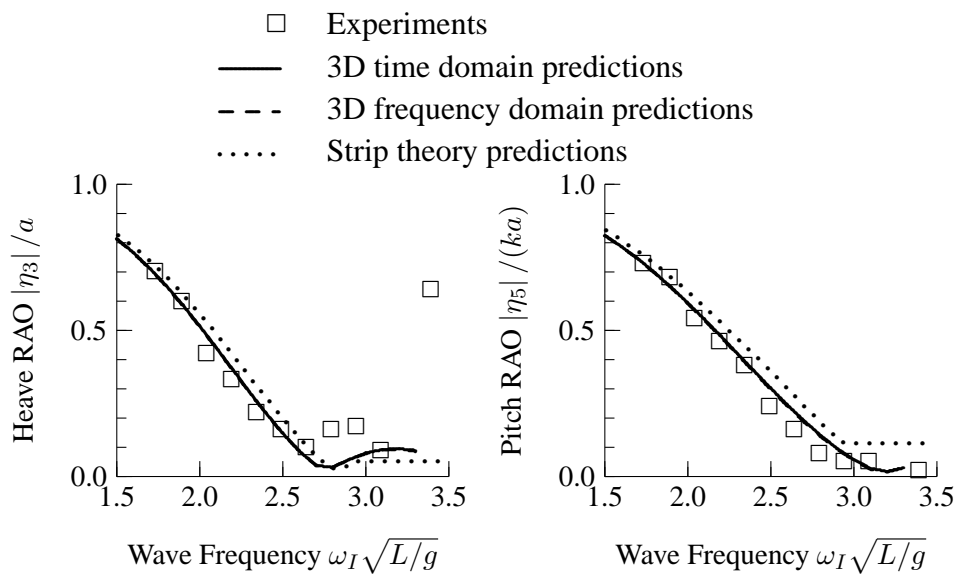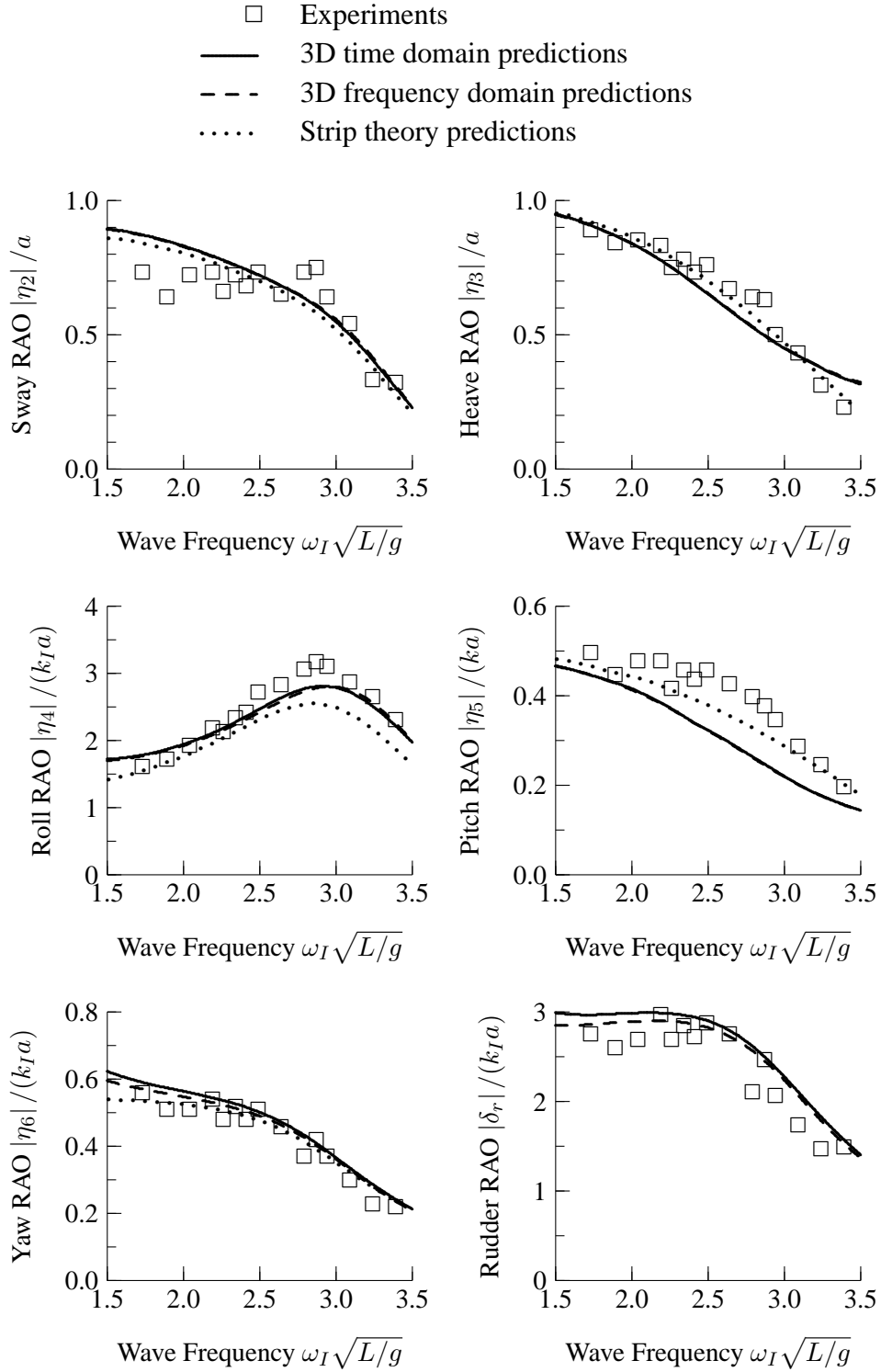
Figure 32: *RAOs for Steered Warship, Stern Quartering Seas at 60 degrees, Froude Number 0.18*
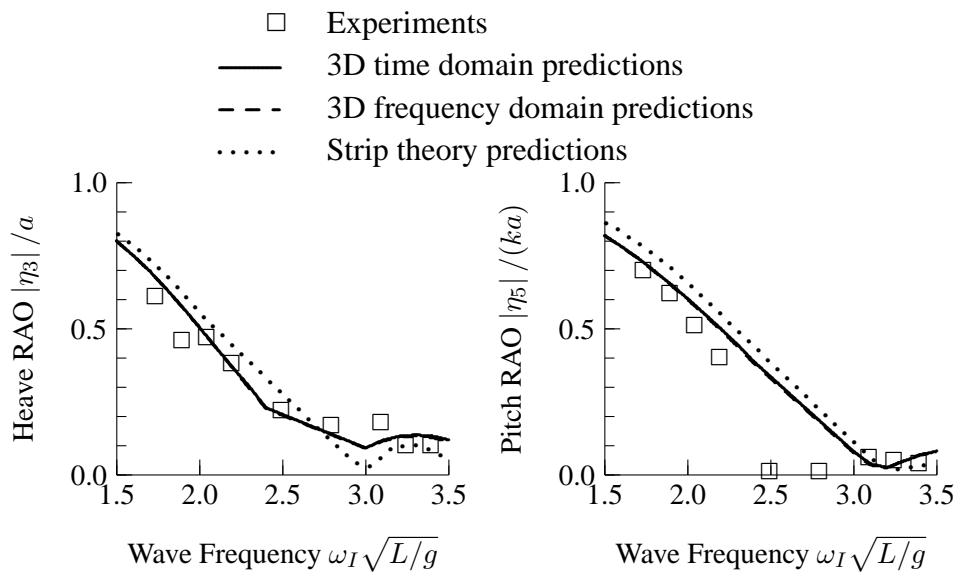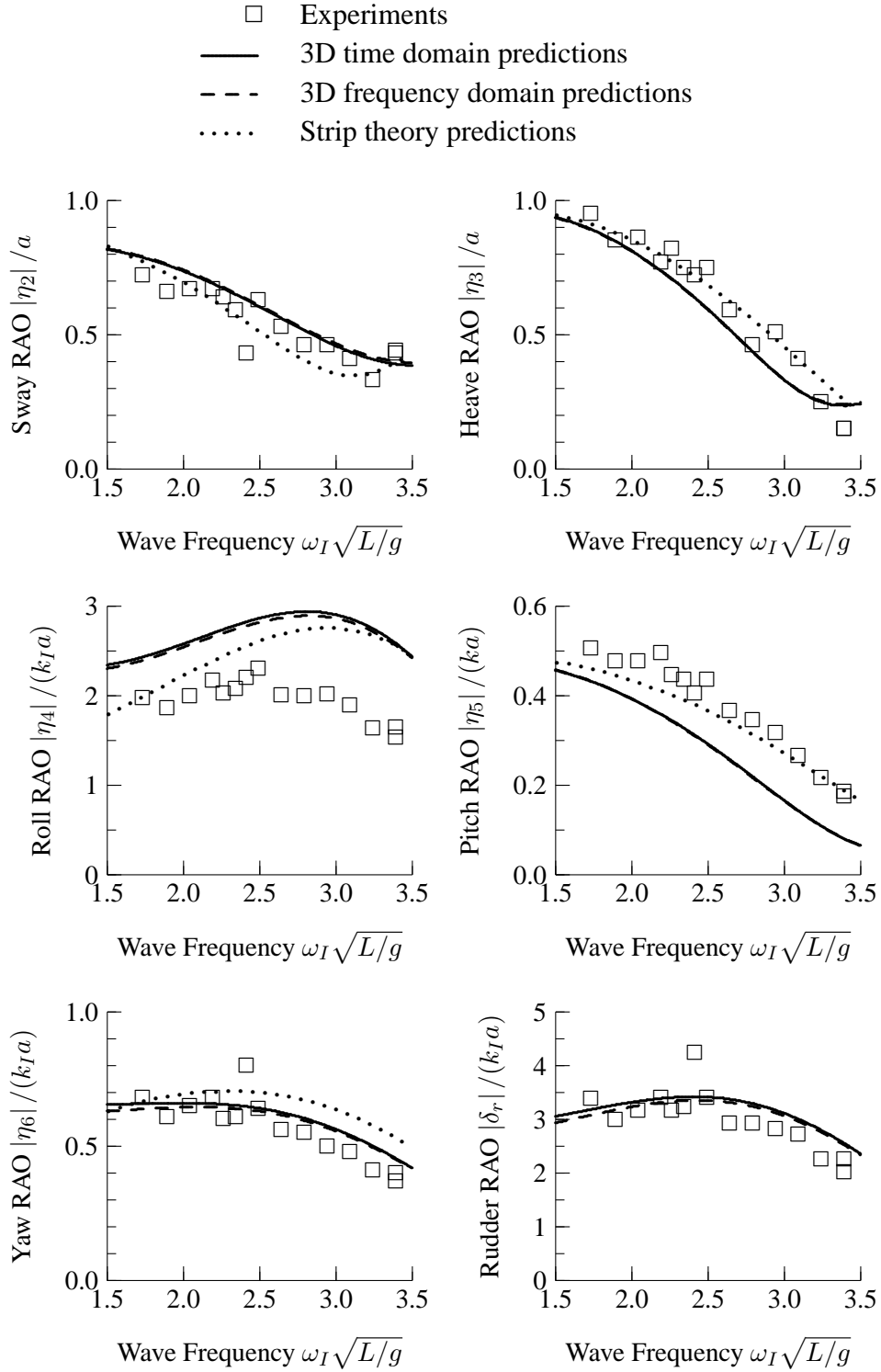
Figure 33: *RAOs for Steered Warship, Stern Quartering Seas at 60 degrees, Froude Number 0.27*
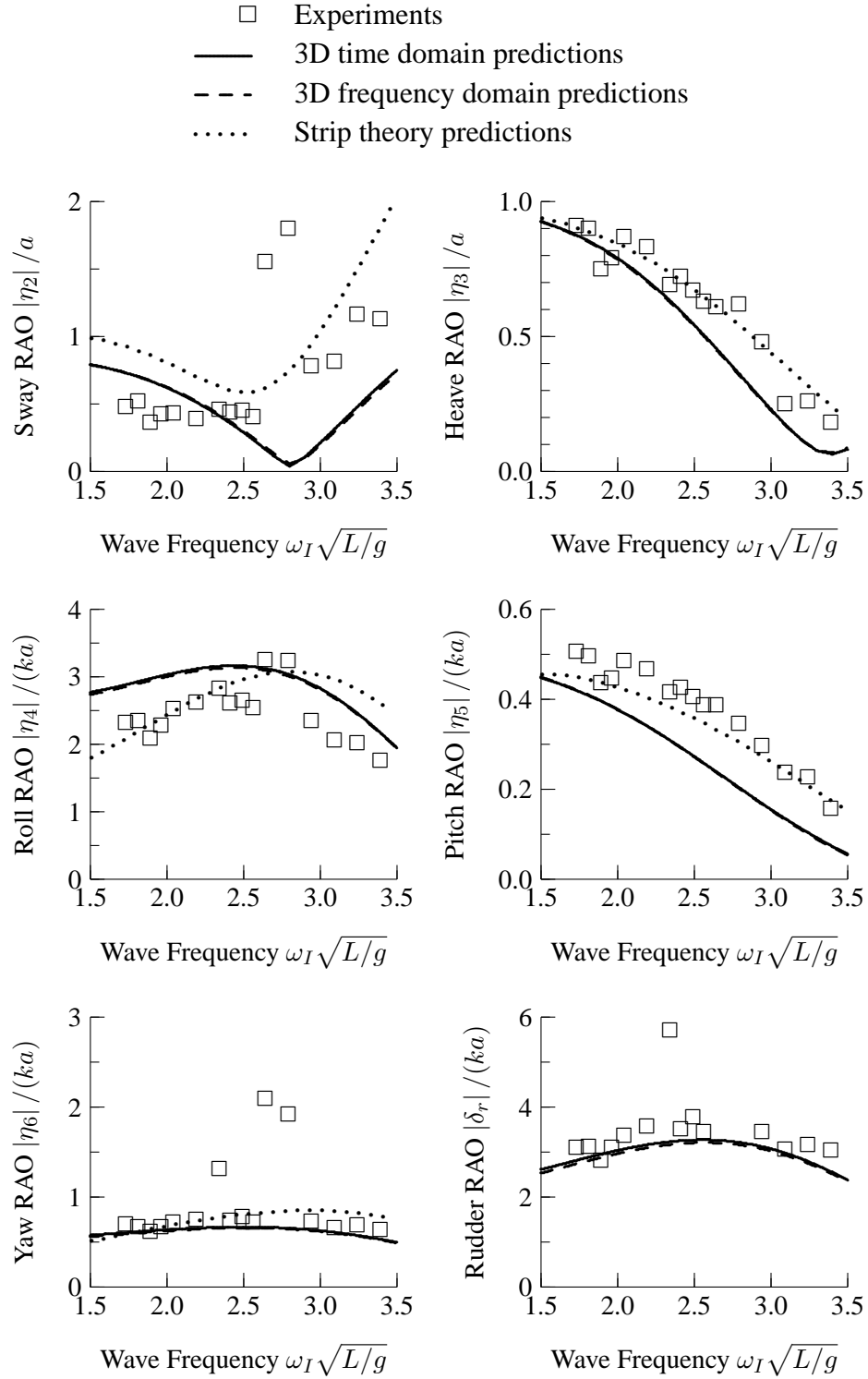
Figure 34: *RAOs for Steered Warship, Stern Quartering Seas at 60 degrees, Froude Number 0.36*
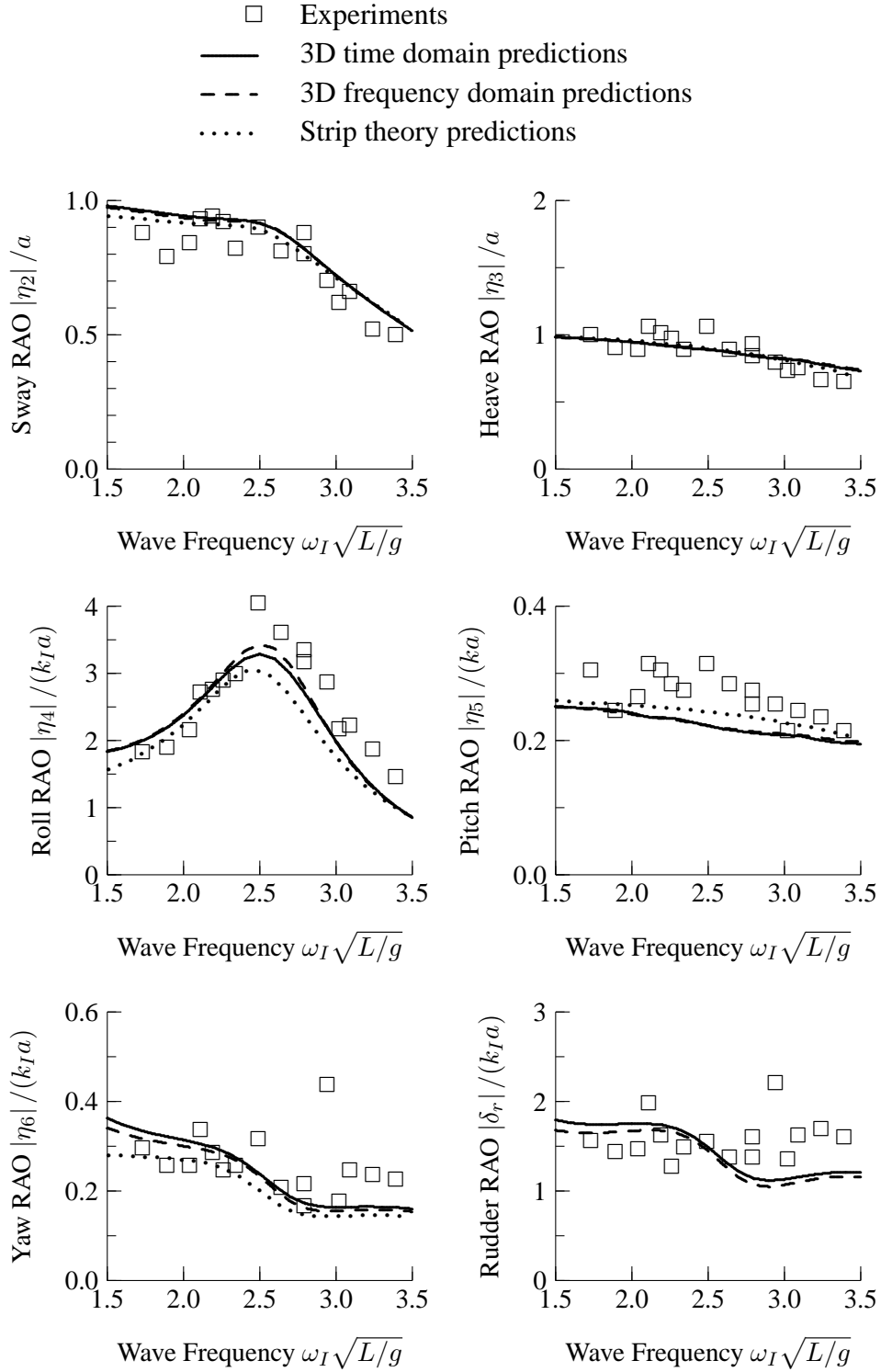
Figure 35: *RAOs for Steered Warship, Stern Quartering Seas at 75 degrees, Froude Number 0.18*
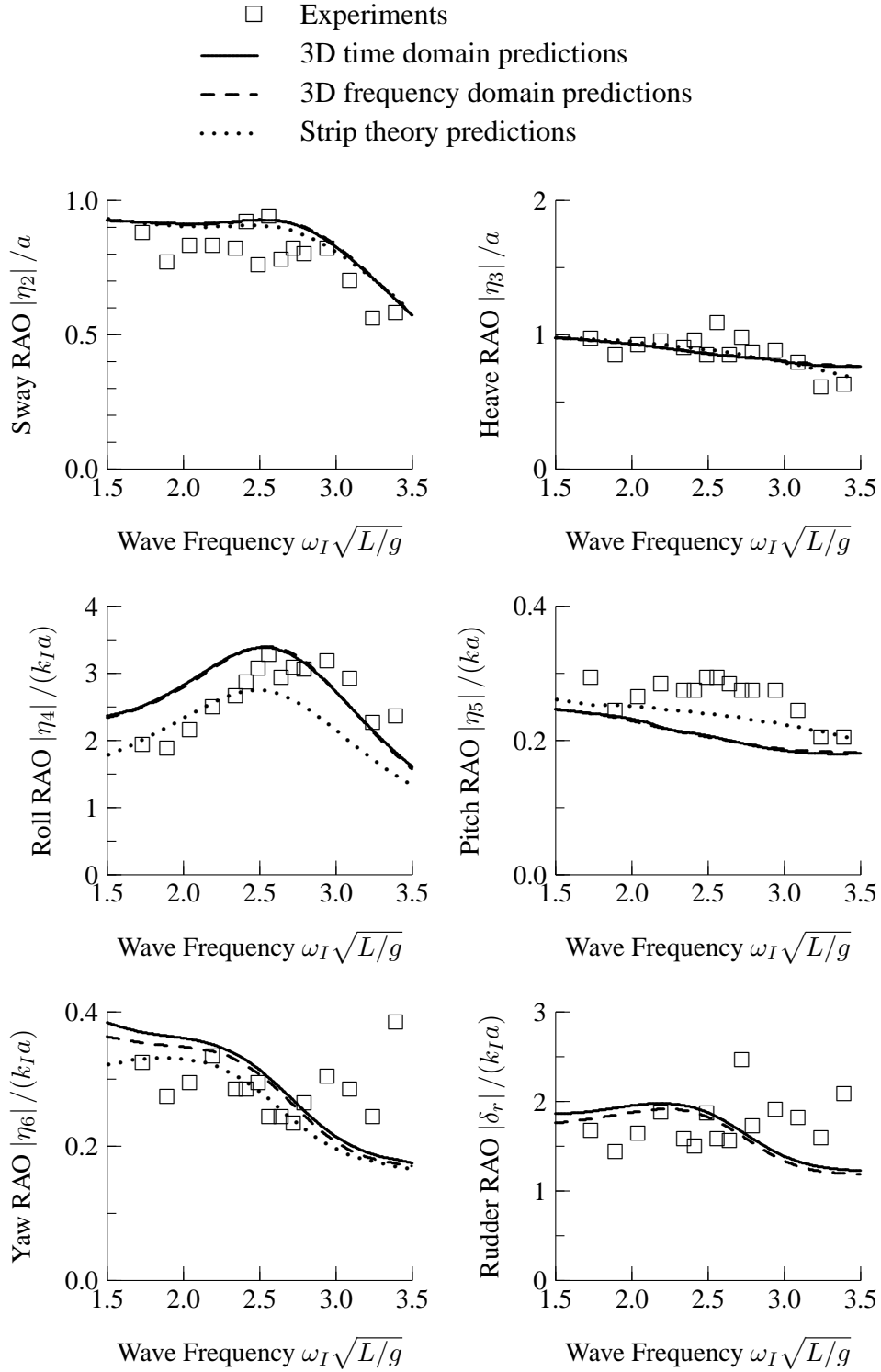
Figure 36: *RAOs for Steered Warship, Stern Quartering Seas at 75 degrees, Froude Number 0.28*
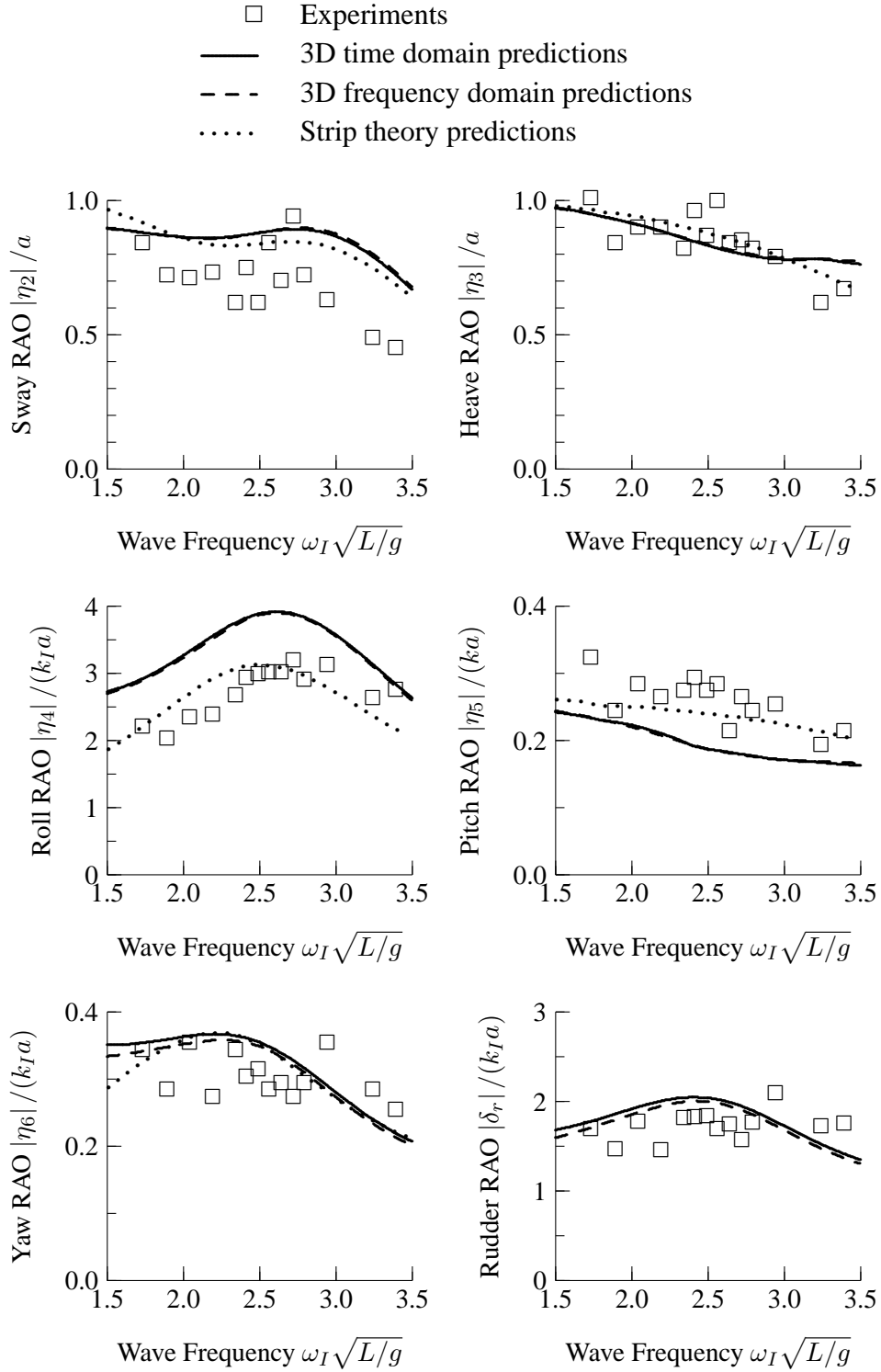
Figure 37: *RAOs for Steered Warship, Stern Quartering Seas at 75 degrees, Froude Number 0.36*
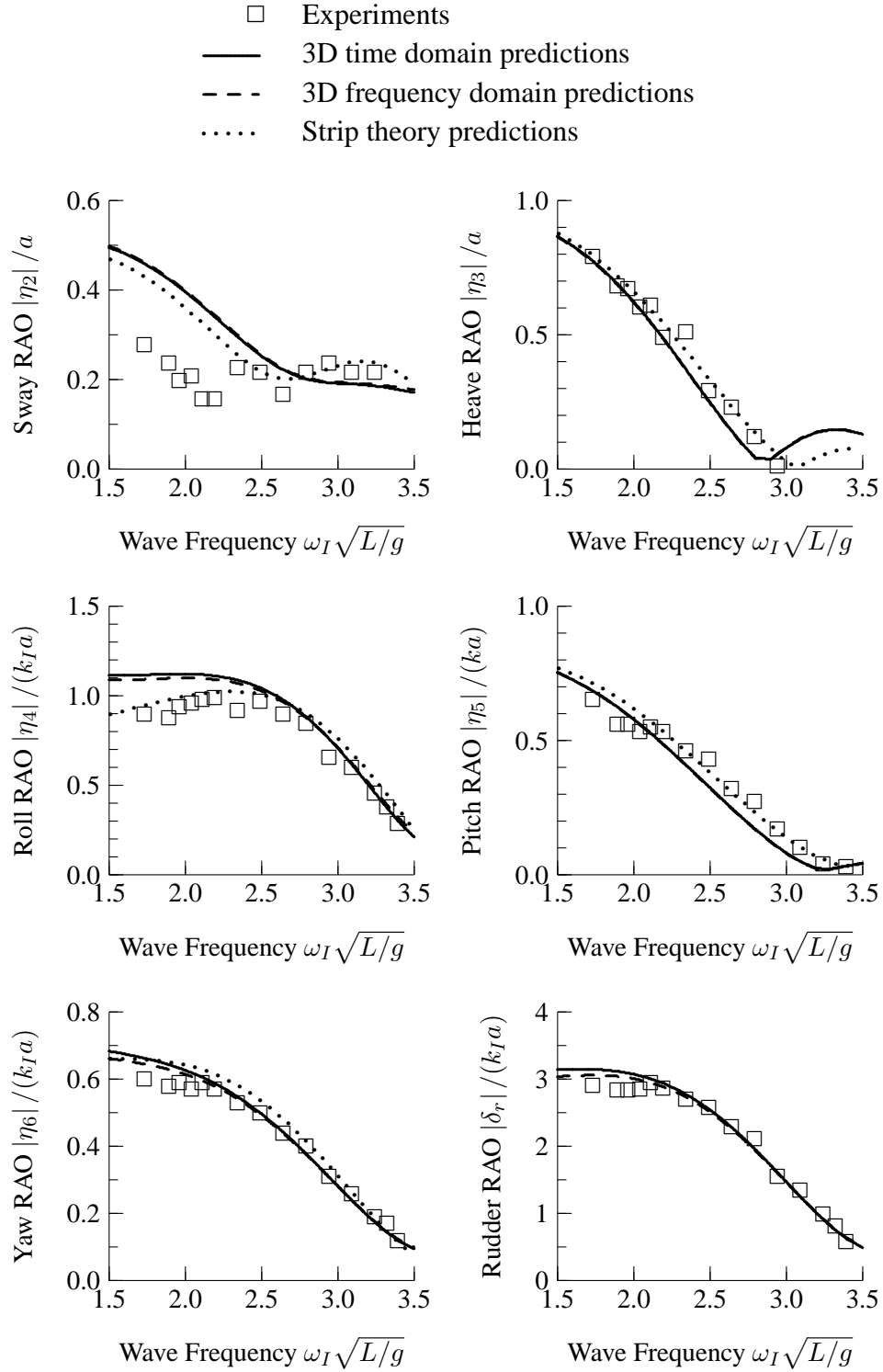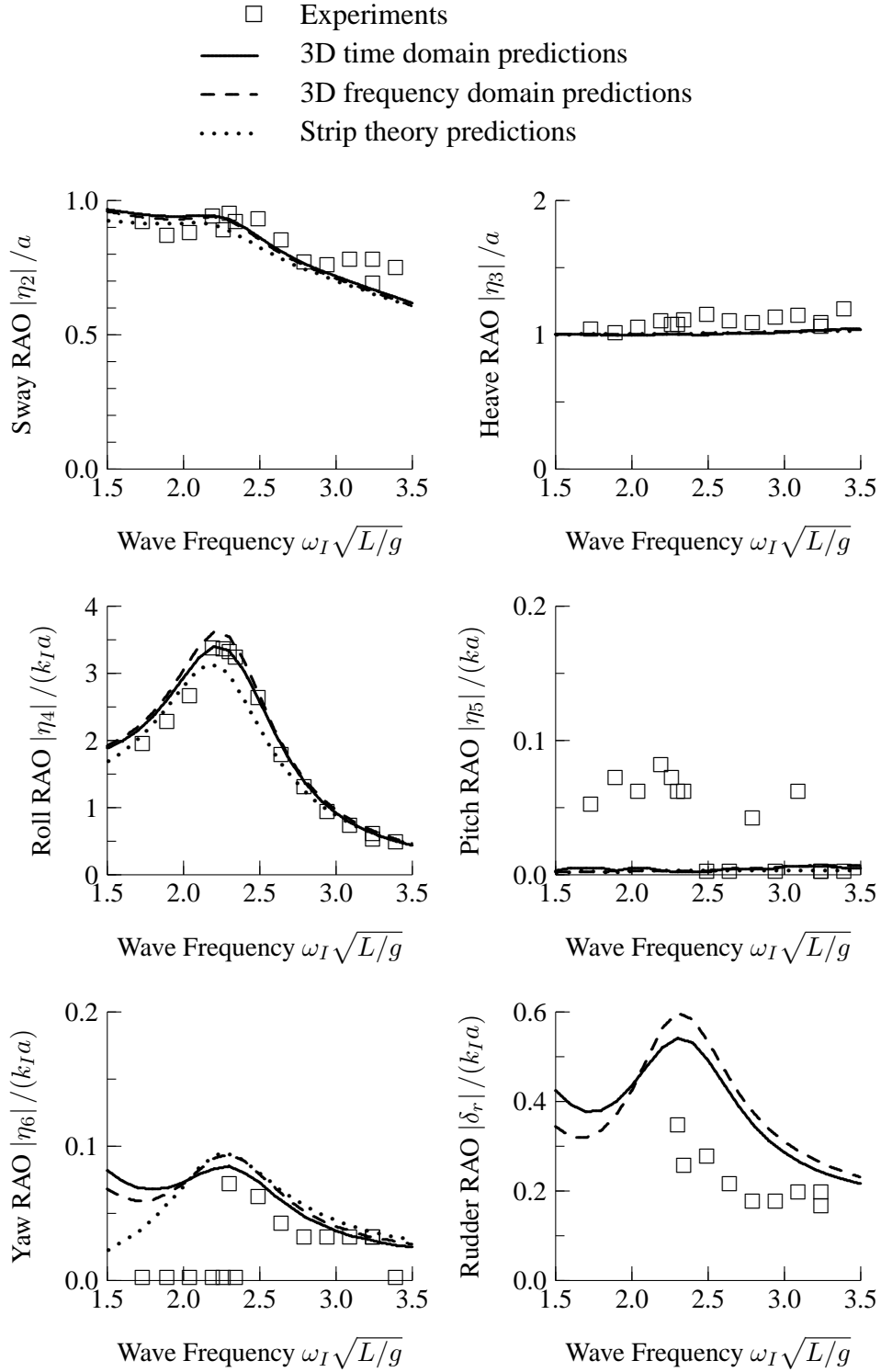
Figure 38: *RAOs for Steered Warship, Stern Quartering Seas at 90 degrees, Froude Number 0.18*

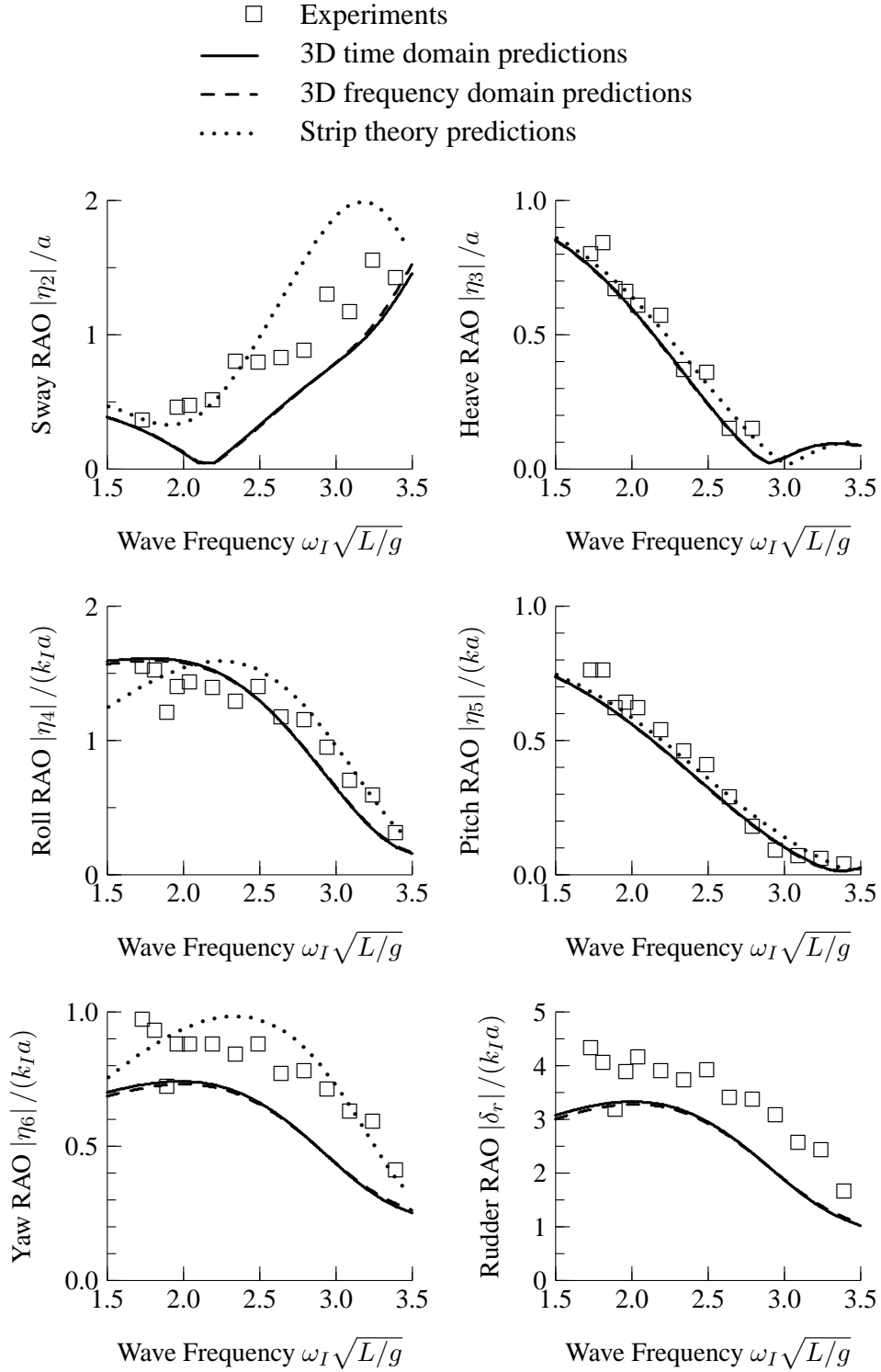**Figure 39:** *RAOs for Steered Warship, Stern Quartering Seas at 90 degrees, Froude Number 0.28*

Figure 40: *RAOs for Steered Warship, Stern Quartering Seas at 90 degrees, Froude Number 0.36*

Figure 41: *RAOs for Steered Warship, Stern Quartering Seas at 120 degrees, Froude Number 0.27*
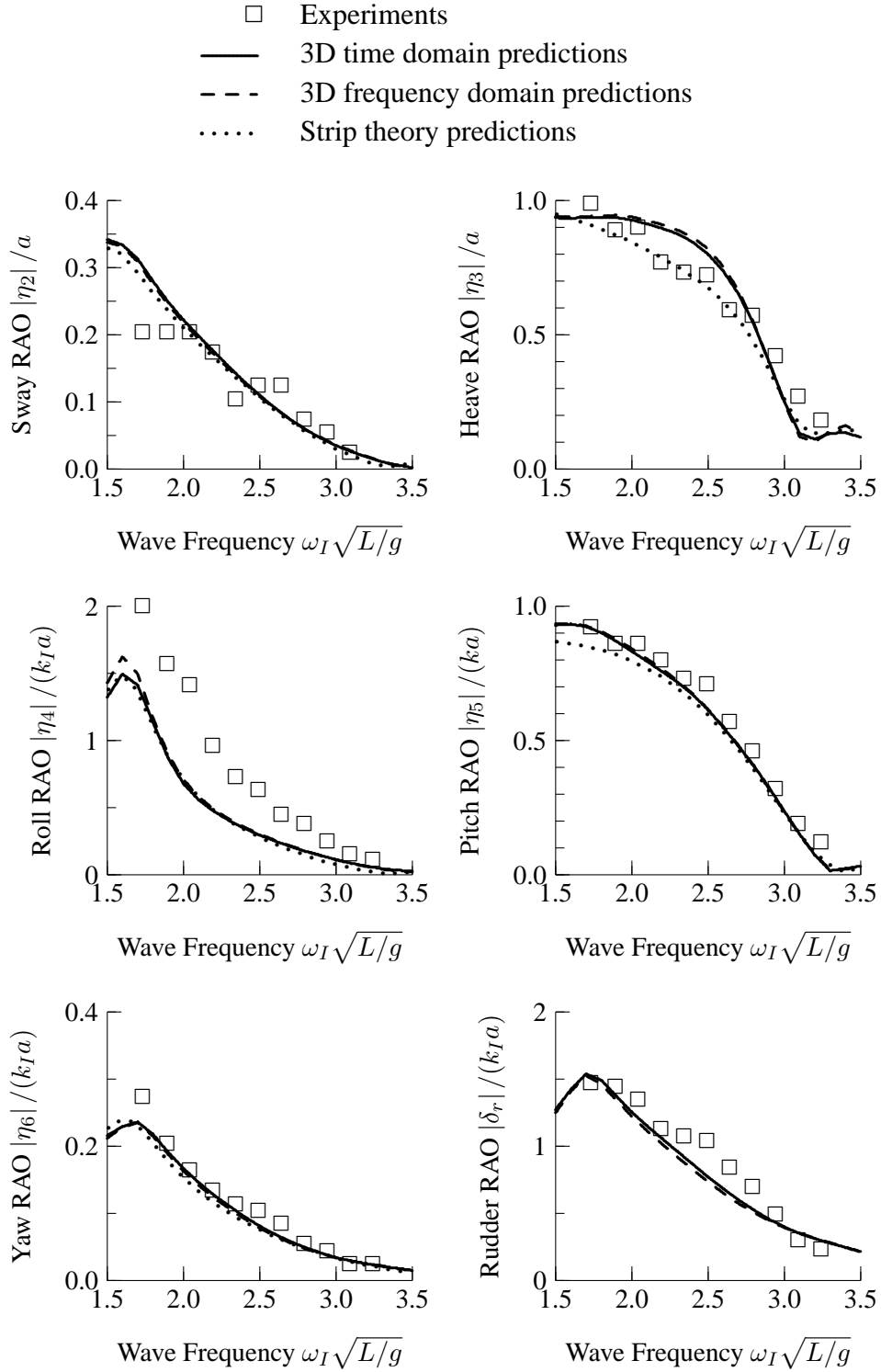
Figure 42: *RAOs for Steered Warship, Stern Quartering Seas at 150 degrees, Froude Number 0.26*
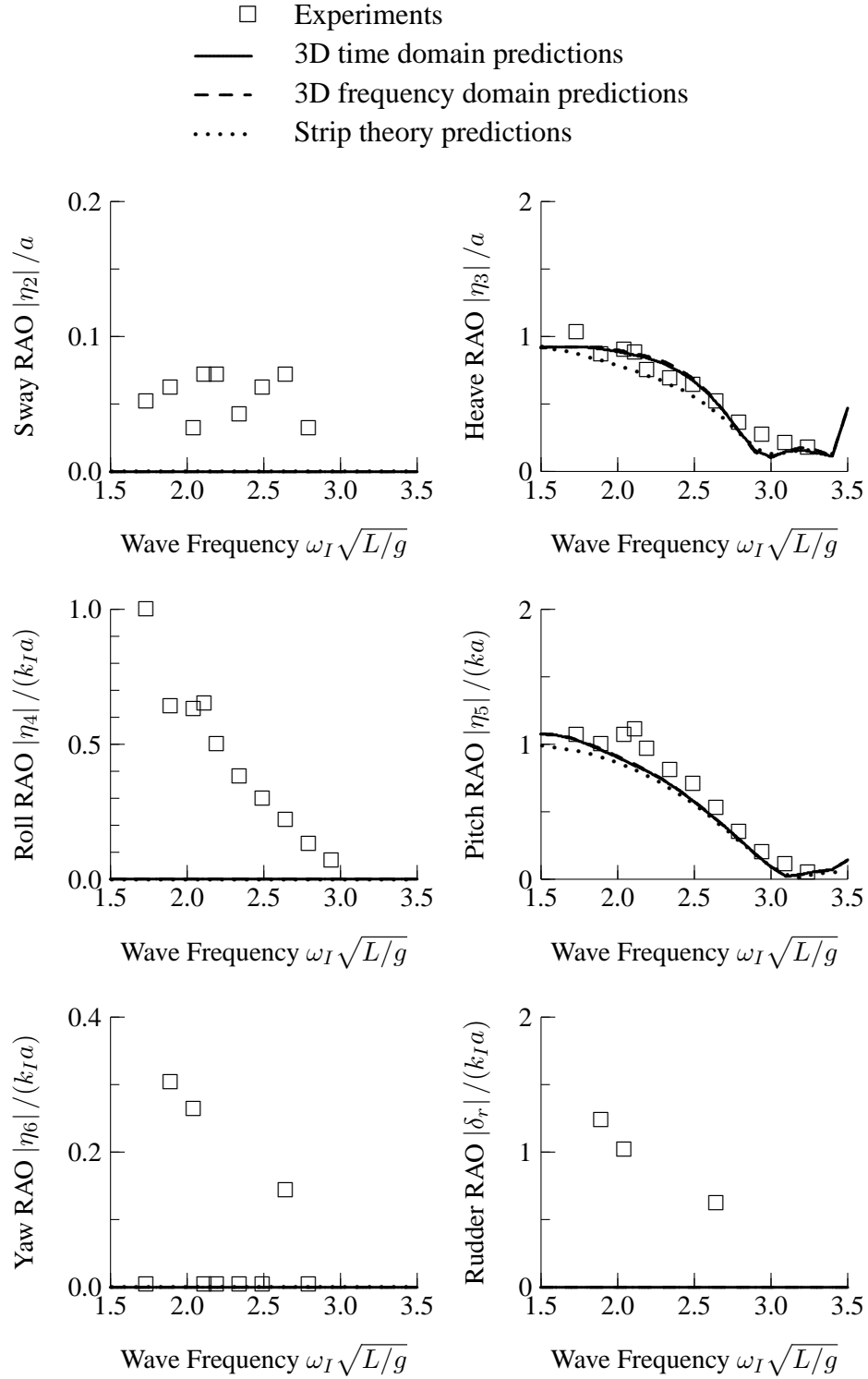
Figure 43: *RAOs for Steered Warship, Stern Quartering Seas at 180 degrees, Froude Number 0.26*
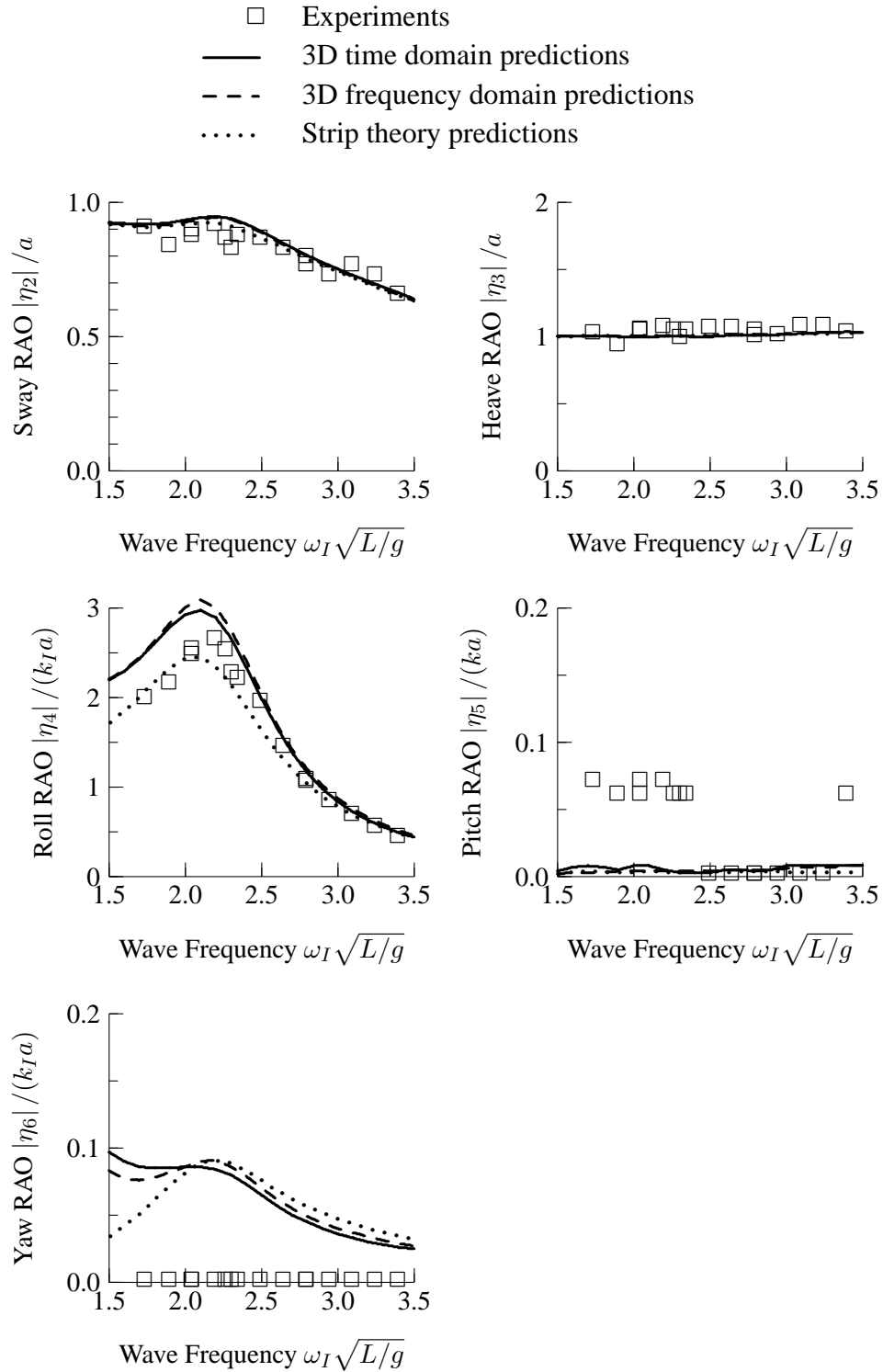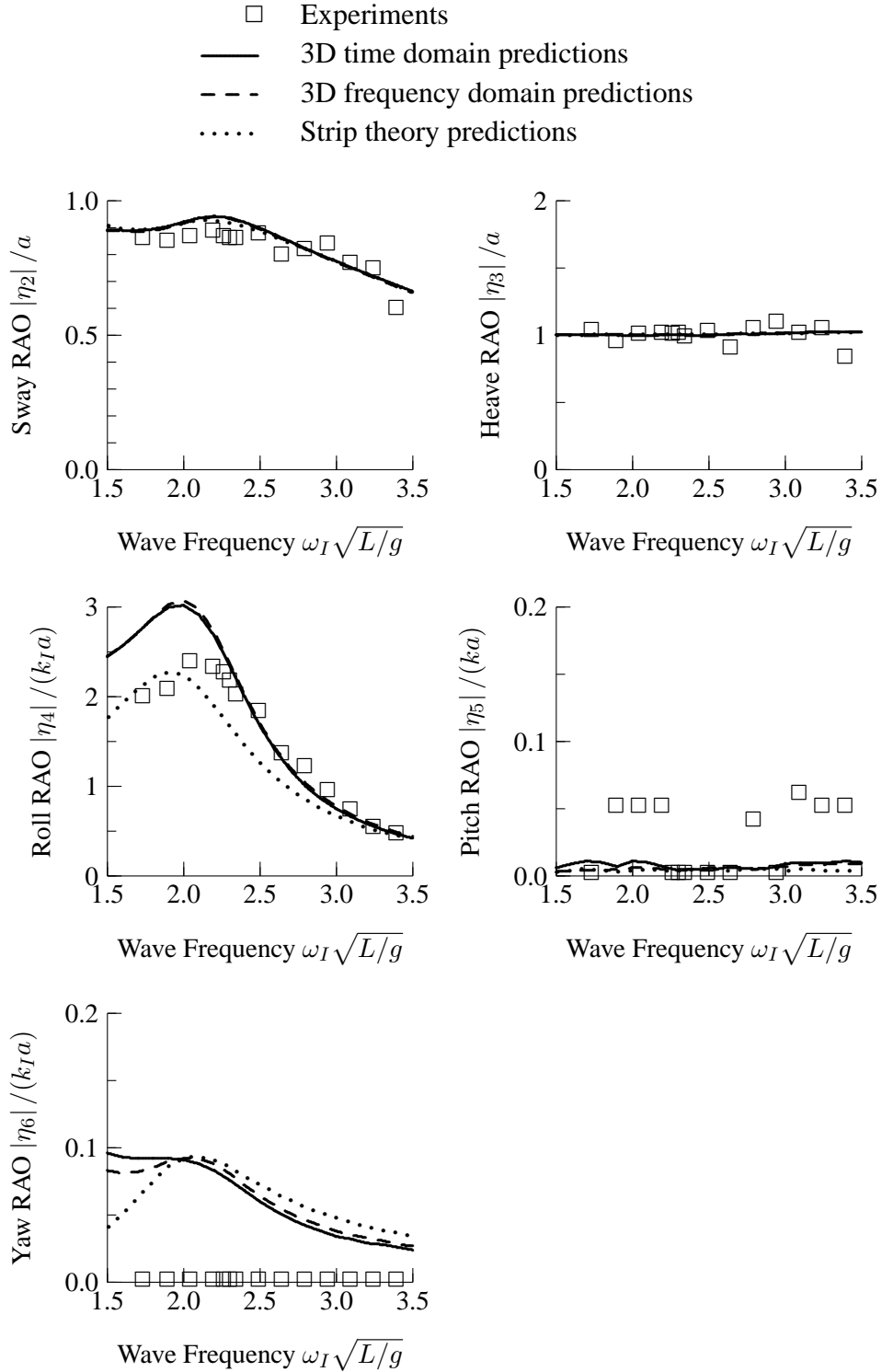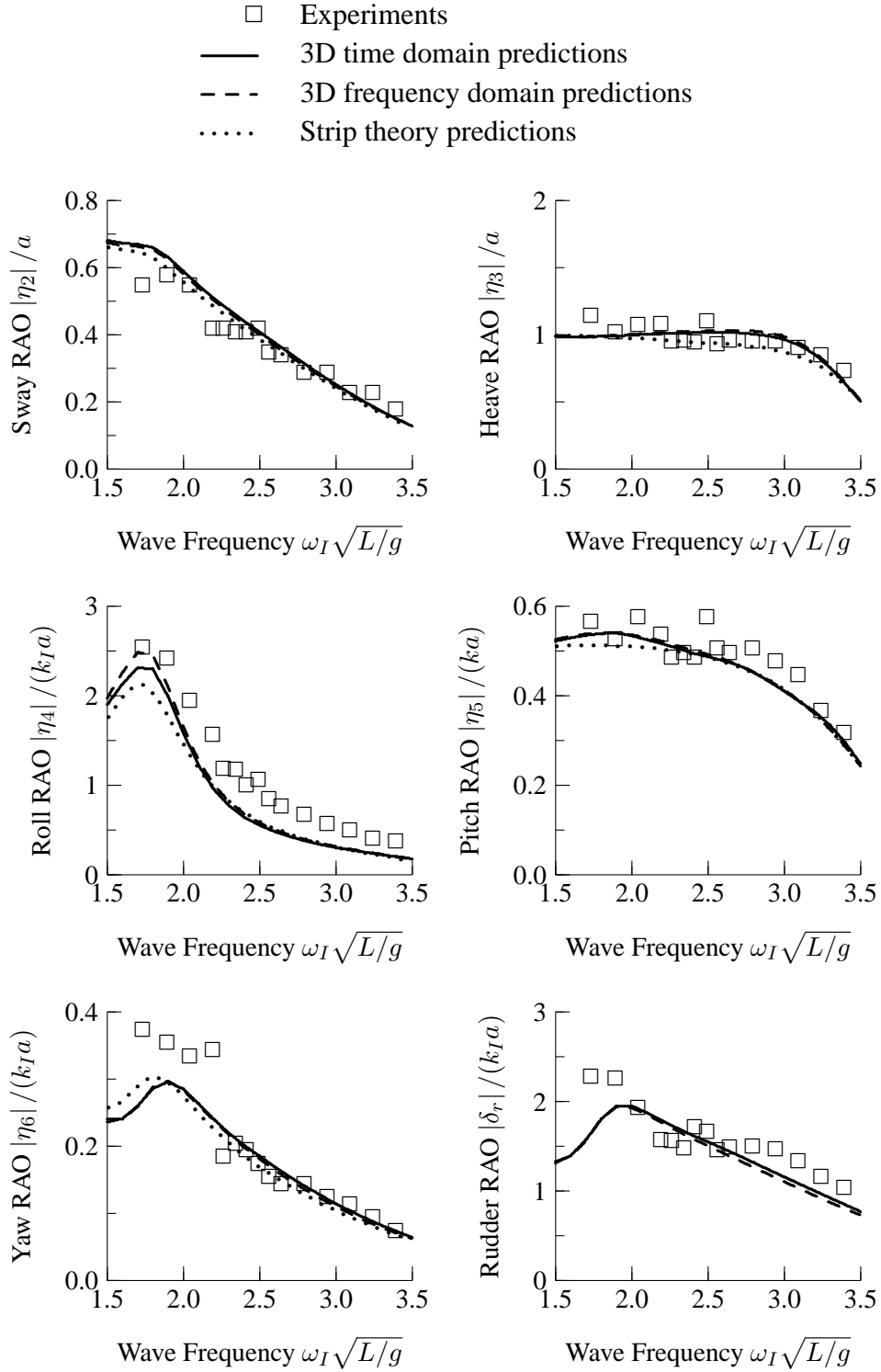
9 Recommendations for Future Work

The ShipMo3D library is being extended to model the motions of a freely maneuvering ship in both calm water and in waves. Hull lift forces are very important for maneuvering ships due to the high angles of attack that can occur; thus, hull lift forces should be added to the ShipMo3D library. Hull lift forces will also influence oscillatory motions in waves.

In the longer term, the ShipMo3D library should be modified such that radiation and diffraction computations can model the influence of hull forward speed on boundary conditions, thus leading to more accurate hull force predictions. This requirement could be satisfied using a forward speed Green function in either the time domain or frequency domain.

10 Conclusions

The ShipMo3D library now includes appendage and viscous forces for predicting ship motions in waves. Modelled appendages can include rudders, bilge keels, skegs, and propeller shaft brackets. Rudder motions can be modelled using a linear autopilot.

The ShipMo3D library can include appendages in hull radiation and diffraction computations using dipole panels on appendage surfaces. Computations for a naval destroyer have shown that inclusion of appendages in hull radiation and diffraction computations has a negligible influence on predicted ship motions.

Motion predictions have been validated with model tests using a steered warship in regular waves. Numerical predictions give generally good agreement with experiments. Heave and pitch predictions are somewhat better than sway, roll, and yaw predictions. Agreement between predictions and experiments tends to decrease as ship speed increases. The current predictions assume low ship speed when evaluating hull radiation and diffraction forces. Furthermore, hull lift forces, which are proportional to ship speed, are neglected in the current predictions.

Near-term work will consider motions of freely maneuvering ships, and will include hull lift forces.

11 Acknowledgement

Paul Crossland of QinetiQ provided geometric data and experimental motion data for the Haslar steered warship model. His contribution is gratefully acknowledged.

References

1. McTaggart, K.A. (2002). Three Dimensional Ship Hydrodynamic Coefficients Using the Zero Forward Speed Green Function. (DRDC Atlantic TM 2002-059). Defence Research and Development Canada - Atlantic.

2. McTaggart, K.A. (2003). Hydrodynamic Forces and Motions in the Time Domain for an Unappended Ship Hull. (DRDC Atlantic TM 2003-104). Defence Research and Development Canada - Atlantic.

3. McTaggart, K.A. (2003). Modelling and Simulation of Seaways in Deep Water for Simulation of Ship Motions. (DRDC Atlantic TM 2003-190). Defence Research and Development Canada - Atlantic.

4. Schmitke, R.T. (1978). Ship Sway, Roll, and Yaw Motions in Oblique Seas. *Transactions, Society of Naval Architects and Marine Engineers*, **86**, 26–46.

5. Himeno, Y. (1981). Prediction of Ship Roll Damping - State of the Art. (Report 239). Department of Naval Architecture and Marine Engineering, University of Michigan.

6. McTaggart, K. and Stredulinsky, D. (2004). Validation of Ship Motion Predictions with Sea Trials Data for a Naval Destroyer in Multidirectional Seas. In *25th Symposium on Naval Hydrodynamics*, St. Johns, Canada.

7. Whicker, L.F. and Fehlner, L.F. (1958). Free Stream Characteristics of a Family of Low Aspect Ratio Control Surfaces for Application to Ship Design. (Report DTRC 933). David Taylor Research Center.

8. McTaggart, K.A. (1997). SHIPMO7: An Updated Strip Theory Program for Predicting Ship Motions and Sea Loads in Waves. (DREA TM 96/243). Defence Research Establishment Atlantic.

9. Newman, J.N. (1977). Marine Hydrodynamics, Cambridge, Massachusetts: MIT Press.

10. Schmitke, R.T. (1978). ROLLRFT - A Fortran Program to Predict Ship Roll, Sway, and Yaw Motions in Oblique Waves, Including the Effects of Rudder, Fin and Tank Roll Stabilizers. (TM 78/G). Defence Research Establishment Atlantic.

11. Sarpkaya, T. and Isaacson, M. (1981). Mechanics of Wave Forces on Offshore Structures, Van Nostrand Reinhold.

12. Crane, C.L., Eda, H., and Landsburg, A. (1989). Principles of Naval Architecture, Volume III, Ch. 9, Controllability. Society of Naval Architects and Marine Engineers.

13. Ikeda, Y., Himeno, Y., and Tanaka, N. (1976). Ship Roll Damping - Frictional Component and Normal Pressure on Bilge Keel. *Journal of Kansai Society of Naval Architects*, Vol. 161.

14. Kato, H. (1966). Effects of Bilge Keels on the Roll Damping of Ships. *Memories of the Defence Academy, Japan*, Vol. 4.

15. McTaggart, K.A. and Stredulinsky, D. (2001). Comparisons of Motions for HMCS NIPIGON with Numerical Predictions. (DREA ECR 2001-156). Defence Research Establishment Atlantic.

16. Lloyd, A.R.J.M. (1989). Seakeeping: Ship Behaviour in Rough Weather, Chichester, England: Ellis Horwood.

17. Graham, R. (1986). SHIPMO3: Improved Viscous Roll Damping Predictions for the SHIPMO Computer Program. (TM 86/212). Defence Research Establishment Atlantic.

18. Tanaka, N. (1960). A Study on the Bilge Keels (Part 4 - On the Eddy-Making Resistance to the Rolling of a Ship Hull. *Journal of the Society of Naval Architects of Japan*, Vol. 109.

19. Ikeda, Y., Himeno, Y., and Tanaka, N. (1978). Components of Roll Damping of Ship at Forward Speed. (Report 00404). Department of Naval Architecture, University of Osaka Prefecture.

20. Kato, H. (1958). On the Frictional Resistance to the Roll of Ships. *Journal of the Society of Naval Architects of Japan*, Vol. 102.

21. Chakrabarti, S.K. (1987). Hydrodynamics of Offshore Structures, Springer-Verlag.

22. Meyerhoff, W.K. (1970). Added Mass of Thin Rectangular Plates Calculated from Potential Theory. *Journal of Ship Research*, **14**, 100–111.

23. Telste, J.G. and Noblesse, F. (1986). Numerical Evaluation of the Green Function of Water-Wave Radiation and Diffraction. *Journal of Ship Research*, **30**(2), 69–84.

24. Garrison, C.J. (1978). Hydrodynamic Loading of Large Offshore Structures. In Zienkiewicz, O.C., Lewis, O.C., and Stagg, K.G., (Eds.), *Numerical Methods in Offshore Engineering*, pp. 87–139. Chichester, England: John Wiley & Sons.

25. Smith, T.C. (1999). T-ADC(X) Maneuvering in Waves Study Using FREDYN. (Report NSWCCD-50-TR-1999\038). NSWCCD.

26. Lutz, M. (2001). Programming Python, Second ed. Sebastopol, CA: O'Reilly & Associates.

27. Lutz, M. and Ascher, D. (1999). Learning Python, Sebastopol, CA: O'Reilly & Associates.

28. Ascher, D., Dubois, P.F., Hinsen, K., Hugunin, J., and Oliphant, T. (2001). Numerical Python. (Technical Report UCRL-MA-128569). Lawrence Livermore National Laboratory. Livermore, California.

29. Lloyd, A.R.J.M. and Crossland, P. (1990). Motions of a Steered Model Warship in Oblique Waves. *Transactions, Royal Institution of Naval Architects*, **132**, 79–98.

Symbols and Abbreviations

A_{ij}^{foil}	foil added mass
A_p^{foil}	foil added mass for motion perpendicular to its surface
A_{ij}^{bk}	bilge keel added mass
A_p^{bk}	added mass of bilge keel for motion perpendicular to its surface
A_x	hull cross-sectional area
a	wave amplitude
a_{Cd}, b_{Cd}	coefficients for estimating bilge keel drag coefficients
a_p	flow acceleration perpendicular to foil
a_y, a_z	flow acceleration components in y and z directions
B	ship beam
B_{ij}^{bk}	bilge keel damping
B_p^{bk}	damping of bilge keel for motion perpendicular to its surface
$B_{44}^{bk-visc}$	bilge keel viscous roll damping
B_{44}^{cr}	critical roll damping
B_{ij}^{foil}	foil damping
B_p^{foil}	foil damping coefficient for motion perpendicular to its surface
$B_{44}^{foil-visc}$	foil viscous roll damping
$B_{44}^{hull-eddy}$	hull roll eddy damping
B_x	hull sectional beam
$[B_{\delta\delta}]$	rudder motion damping matrix
$[B_{\delta\eta}]$	rudder-ship motion damping coupling matrix
$[B_{\eta\eta}]$	ship motion damping matrix
C_{ij}^{bk}	ship motion stiffness from bilge keel
C_d	drag coefficient
C_{ij}^{foil}	ship motion stiffness from foil
C_{eddy}^{hull}	hull eddy damping coefficient
C_f^{hull}	hull skin friction coefficient
C^{lift}	lift coefficient
C_δ^{rudder}	force stiffness coefficient for rudder deflection
$C_{i\delta}^{rudder}$	rudder deflection stiffness coefficient for ship motion mode i
$[C_{\delta\delta}]$	rudder motion stiffness matrix
$[C_{\delta\eta}]$	rudder-ship motion stiffness coupling matrix
$[C_{\eta\eta}]$	ship motion stiffness matrix
$\bar{c}$	mean chord length
c_{root}	chord length at root
c_{tip}	chord length at tip
F_j^{bk}	wave excitation force on bilge keel for mode j
$F^{bk-lift}$	lift force on bilge keel

$F^{bk-visc}$	viscous force on bilge keel
$F^{foil-visc}$	viscous force on foil
$F_4^{foil-visc}$	foil viscous roll moment
$F^{hull-eddy}$	hull eddy force
$F^{hull-skin}$	hull skin friction force
$\{F_\eta\}$	ship motion excitation force vector
$G^{dipole}(\vec{x}, \vec{x}_d, k_e)$	Green function for dipole
$G(\vec{x}, \vec{x}_d, k_e)$	Green function for source
$\overline{G}_0(\vec{x}, \vec{x}_d, k_e)$	zero frequency Green function for source
$\widetilde{G}_0$	frequency dependent term of Green function relative to zero frequency Green function
$\overline{G}_\infty(\vec{x}, \vec{x}_d, k_e)$	infinite frequency Green function for source
$\overline{GM}$	metacentric height
g	gravitational acceleration
h	non-dimensional horizontal distance from field point to source
$J_0(h)$	Bessel function of the first kind of order zero
$J_1(h)$	Bessel function of the first kind of order one
$\overline{KG}$	height of centre of gravity above baseline
k_e	encounter wavenumber
k_I	incident wavenumber
$k_{\delta j}^a$	rudder deflection acceleration gain for ship motion mode j
$k_{\delta j}^d$	rudder deflection displacement gain for ship motion mode j
$k_{\delta j}^v$	rudder deflection velocity gain for ship motion mode j
L_{pp}	ship length between perpendiculars
$[M_{\delta\delta}^e]$	rudder motion inertia matrix
$[M_{\delta\eta}^e]$	rudder-ship motion inertia coupling matrix
$[M_{\eta\eta}^e]$	effective ship mass matrix
n^{dipole}	normal vector for dipole surface
n_x, n_y, n_z	x, y, and z components for normal pointing outward from hull
n_4	hull roll normal
R	distance from field point to source
R_{xy}	horizontal distance from field point to source
R_{bilge}	hull bilge radius
$\widetilde{R}_0(h, v)$	term for evaluation of frequency dependent Green function
R_1	distance from field point to source image
$\widetilde{R}_1(h, v)$	term for evaluation of frequency dependent Green function
Re^{foil}	foil Reynolds number
r_{BK}	roll radius from ship centre of gravity to bilge keel
r_l	effective roll radius for lift forces
$\widetilde{r}_l^2$	effective square of roll radius squared for lift forces
$\widetilde{r}_v^3$	effective cube of roll moment arm for viscous forces

r_{xx}	roll radius of gyration
r_{yy}	pitch radius of gyration
r_{zz}	yaw radius of gyration
S	foil area
S_{dipole}	dipole surface
s	span
s_{max}	maximum span
T_{mid}	midships draft
T_x	hull sectional draft
t_s	trim by stern
U	ship forward speed
u_p	flow velocity perpendicular to foil
u_y, u_z	flow velocity components in y and z directions
V	flow velocity
V_p	flow velocity perpendicular to foil
v	non-dimensional vertical distance from field point to source image
x, y, z	coordinates in translating earth axes
$\overline{x}, \overline{y}, \overline{z}$	coordinates of foil centroid
$\vec{x}$	location in space
x_{aft}, x_{fore}	aft and forward x limits for long low-aspect ratio foil
$\vec{x}_d$	dipole location
x_{FP}	x coordinate of ship forward perpendicular
x^{foil}	x coordinate of foil
$\vec{x}_s$	source location
α	foil angle of attack
β	wave direction relative to ship
Γ	foil dihedral angle
ΔU^{bk}	local flow velocity correction at bilge keel
ΔU^{foil}	local flow velocity correction at foil
$\Delta \hat{\eta}_4^{damping}$	increment in guess for roll damping amplitude
δ^{rudder}	rudder deflection angle
δ_b	hull boundary layer thickness
δ_C^{rudder}	command rudder deflection angle
$\epsilon^{tol}(\hat{\eta}_4)$	tolerance for roll damping amplitude
ζ_δ	damping ratio for rudder control system
η_j	ship motion displacement for mode j
$\dot{\eta}_j$	ship motion velocity for mode j
$\hat{\eta}_4$	roll amplitude
$\hat{\dot{\eta}}_4$	roll velocity amplitude
ν	water kinematic viscosity
μ	dipole strength
ρ	water density

υ	local roll velocity ratio
ϕ	velocity potential
ω_e	wave encounter frequency
ω_δ	natural frequency for rudder control system
$\triangle$	ship mass displacement

DOCUMENT CONTROL DATA
(Security classification of title, body of abstract and indexing annotation must be entered when document is classified)

1. ORIGINATOR (the name and address of the organization preparing the document). Defence R&D Canada - Atlantic	2. SECURITY CLASSIFICATION (overall security classification of the document including special warning terms if applicable) UNCLASSIFIED

3. TITLE (The complete document title as indicated on the title page. Its classification should be indicated by the appropriate abbreviation (S,C,R or U) in parentheses after the title.) Appendage and Viscous Forces for Ship Motions in Waves

4. AUTHORS (Last name, first name, middle I. If military, show rank, e.g. Doe, Maj. John E.) McTaggart, Kevin A.

5. DATE OF PUBLICATION (month and year of publication of document) September 2004	6a. NO. OF PAGES (total including Annexes, Appendices, etc). 80	6b. NO. OF REFS (total cited in document) 29

7. DESCRIPTIVE NOTES (The category of the document, e.g. technical report, technical note or memorandum. If appropriate, enter the type of report, e.g. interim, progress, summary, annual or final.) Technical Memorandum

8. SPONSORING ACTIVITY (the name of the department project office or laboratory sponsoring the research and development. Include address). Defence R&D Canada - Atlantic, PO Box 1012, Dartmouth, NS, Canada B2Y 3Z7

9a. PROJECT OR GRANT NO. (If appropriate, the applicable research and development project or grant number under which the document was written.) 11GK12	9b. CONTRACT NO. (if appropriate, the applicable number under which the document was written).

10a. ORIGINATOR'S DOCUMENT NUMBER (the official document number by which the document is identified by the originating activity. This number must be unique.) DRDC Atlantic TM 2004-227	10b. OTHER DOCUMENT NOs. (Any other numbers which may be assigned this document either by the originator or by the sponsor.)

11. DOCUMENT AVAILABILITY (any limitations on further dissemination of the document, other than those imposed by security classification) (X) Unlimited distribution ( ) Defence departments and defence contractors; further distribution only as approved ( ) Defence departments and Canadian defence contractors; further distribution only as approved ( ) Government departments and agencies; further distribution only as approved ( ) Defence departments; further distribution only as approved ( ) Other (please specify):

12. DOCUMENT ANNOUNCEMENT (any limitation to the bibliographic announcement of this document. This will normally correspond to the Document Availability (11). However, where further distribution (beyond the audience specified in (11) is possible, a wider announcement audience may be selected.)

13. ABSTRACT (a brief and factual summary of the document. It may also appear elsewhere in the body of the document itself. It is highly desirable that the abstract of classified documents be unclassified. Each paragraph of the abstract shall begin with an indication of the security classification of the information in the paragraph (unless the document itself is unclassified) represented as (S), (C), (R), or (U). It is not necessary to include here abstracts in both official languages unless the text is bilingual).

This report describes the prediction of appendage and viscous forces in DRDC Atlantic's ShipMo3D library for ship motions in waves. Previously, the ShipMo3D library considered only hull forces due to potential flow. Inclusion of appendage and viscous forces is essential for accurate prediction of ship sway, roll, and yaw motions. Appendage forces are caused by added mass, lift, and viscous effects. Hull viscous forces are also important and are included in the present treatment. This report introduces a method for including appendages in hull radiation and diffraction computations by representing appendages using dipole panels. Computations for a naval destroyer have indicated that inclusion of appendages in hull radiation and diffraction computations has a negligible effect on predicted motions; thus, hull and appendage forces can be evaluated separately without affecting accuracy of motion predictions. Comparisons of predictions with experiments for a steered warship model in regular waves show good agreement. Future work will incorporate hull lift forces in ship motion predictions.

14. KEYWORDS, DESCRIPTORS or IDENTIFIERS (technically meaningful terms or short phrases that characterize a document and could be helpful in cataloguing the document. They should be selected so that no security classification is required. Identifiers, such as equipment model designation, trade name, military project code name, geographic location may also be included. If possible keywords should be selected from a published thesaurus. e.g. Thesaurus of Engineering and Scientific Terms (TEST) and that thesaurus-identified. If it not possible to select indexing terms which are Unclassified, the classification of each should be indicated as with the title).

lift
roll
sway
seakeeping
ship motions
yaw

This page intentionally left blank.

Defence R&D Canada

Canada's leader in defence
and national security R&D

R & D pour la défense Canada

Chef de file au Canada en R & D
pour la défense et la sécurité nationale

DEFENCE **R&D** DÉFENSE

www.drdc-rddc.gc.ca